EXPERIMENTAL AND COMPUTATIONAL STUDIES ON AN ALPHA TYPE STIRLING ENGINE FOR COMBINED HEAT AND POWER APPLICATIONS

A THESIS

submitted by

N AJEY

for the award of the degree

of

MASTER OF SCIENCE

(by Research)

DEPARTMENT OF MECHANICAL ENGINEERING
INDIAN INSTITUTE OF TECHNOLOGY MADRAS.

MARCH 2017

Dedicated to my wife

Dayani P

THESIS CERTIFICATE

This is to certify that the thesis titled **EXPERIMENTAL AND COMPUTATIONAL STUDIES ON AN ALPHA TYPE STIRLING ENGINE FOR COMBINED HEAT AND POWER APPLICATIONS**, submitted by **N AJEY**, to the Indian Institute of Technology, Madras, for the award of the degree of **Master of Science**, is a bona fide record of the research work done by him under our supervision. The contents of this thesis, in full or in parts, have not been submitted to any other Institute or University for the award of any degree or diploma.

Prof. T Sundararajan
Research Guide
Professor
Dept. of Mechanical Engineering
IIT-Madras, 600 036

Dr. S Varunkumar
Research Guide
Assistant Professor
Dept. of Mechanical Engineering
IIT-Madras, 600 036

Place: Chennai

Date:

ACKNOWLEDGEMENTS

I am immensely grateful to my guide Prof. T Sundararajan and co-guide, Dr. Varunkumar S for their valuable guidance and unparalleled support offered towards my research. Their unsurpassed knowledge and beneficial advice catalysed to achieve the desired results.

I am indebted to the Head of the department, Prof. BVSSS Prasad and my Graduate Test Committee members, Prof. A Mani, Prof. Krishna Vasudevan for their valuable comments and suggestions on the research work.

I greatly acknowledge the funding received from Industrial Consultancy & Sponsored Research (IC&SR) to carry out the research under Exploratory Research Project (ERP) scheme. I extend my gratitude to the personnel of High Performance Computing Environment (HPCE) facility at IIT Madras for providing access to the computational facility. I would like to thank Mr. Ajit Kumar for helping me with fabrication.

I am grateful to my friend Mr. Mahesh J for assisting me in almost every aspect my of research. My appreciation goes out to the field research members Ms. Mani Kalyani, Ms. Priyanka, Mr. VM Jaganathan, Mr. Syed Mughees Ali for their invaluable contribution towards my thesis. I am thankful to Mr. Mohammad Zaved Siddiqui and Mr. Vishal Wadhai for their invaluable assistance regarding coding.

I thank my family and friends for the moral support throughout the research.

ABSTRACT

KEYWORDS: Stirling engine; alpha type; dimensional analysis; CFD; combined heat and power;

This thesis constitutes fundamental experimental and numerical studies on Stirling engines. The principal aim is to develop a CFD based tool for design and development of Stirling engines for domestic scale combined heating and power generation (a few 100 W) applications. Such systems using renewable sources like biomass and solar are attractive options to meet the energy demands (power, heating and cooling) in areas with limited or no access to grid.

Lack of a unifying theoretical framework for understanding the performance of these engines is a major hurdle in developing new designs. While a number of attempts have been made in the analysis of a given engine design that can be found reported in literature they are of very little use to design and develop a new engine. The principal limitation is due to lack of data on external heat transfer processes. Therefore a V-type air engine was designed and developed as a part of this work mainly for measuring external heat transfer parameters and frictional power. A lab scale α-type Stirling engine is developed from a single stage two cylinder compressor. The design consists of a shell and tube heat exchanger for hot and cold side with a wire mesh regenerator connecting the two. A flameless LPG combustion chamber is used for heating and water is used for cooling. By cranking the engine at various speeds using a 1 hp DC motor, heat transfer to the working fluid is estimated using temperature measurements at inlet and exit of the heat exchanger with thermocouples. The frictional power of the engine is calculated by measuring current and voltage across the motor at various speeds. The experimental V-engine is taken as the base configuration and the flow, heat transfer and piston motion is simulated in ANSYS-Fluent. The engine is modeled as a 2D axi-symmetric configuration. The expansion and compression piston dimensions - stroke (S) and bore, are 60 mm respectively, corresponding to the lab engine. The wire mesh regenerator of length 50 mm and diameter 50 mm is modeled as a porous medium with a porosity of

0.86 and permeability of 10^{-7} m^2. Based on the heater and cooler tube diameters (d_e) and average piston speed (U_p), the Reynolds number of the flow was estimated to be below 2000 and hence taken as laminar. The heat transfer is modeled by a convective heat transfer boundary condition to account for the flow of hot gases past the heater tubes from an LPG flameless combustor and cooling water past the cooler tubes like in the experimental engine. The numerical values for the heat transfer coefficient were estimated to be about 10 W/m^2-K for the heater side and 50 W/m^2-K for the cooler side from an energy balance calculation using the experimentally determined temperatures at heater and cooler inlets and outlets.

The ratio of the convective to diffusive heat transfer time scales given by,

$$\tau = \left[\frac{p_{ref}}{RT_c}\right]\left[\frac{SN_s d_e}{30\mu_0}\right]\left[\frac{d_e}{L_e}\right]$$

where, p_{ref} is the operating pressure, T_c is the reference sink temperature, R is the specific gas constant, S is the stroke, N is the speed of the engine in rpm, μ_0 is the dynamic viscosity of the working fluid, d_e is the diameter of the heater, L_e is the heater length, is identified as the governing non-dimensional parameter. Grid independent solutions were obtained for τ values ranging from 0 to 30 for five sets of heater and cooler lengths, namely, 65, 130, 260, 390 and 520 mm, engine speeds from 100 to 1000 rpm, operating pressure 1, 5 & 10 bar and three working fluids namely air, helium and hydrogen (72 simulations in total). The engine characteristics, namely, indicated efficiency and specific power variation for a range of geometries, speeds, operating pressures and working medium are shown to follow a universal function of the dimensional group τ. Results show that all data, irrespective of the working fluid or operating pressure, falls in a narrow band and follows similar trend. Based on this feature an improved design procedure is set out.

TABLE OF CONTENTS

LIST OF TABLES

LIST OF FIGURES

NOTATION

C_p	Specific heat at constant pressure, kJ/kg-K
c_w	Heat capacity, kJ/kg
d_e	heater tube diameter, m
d_c	cooler tube diameter, m
d_r	regenerator tube diameter, m
d_w	regenerator wire diameter, m
h_c	cooler external heat transfer coefficient, W/m^2-K
h_e	heater external heat transfer coefficient, W/m^2-K
k_0	Thermal conductivity of gas at 300K, W/m-K
L_c	Cooler tube length, m
L_e	Heater tube length, m
L_r	Regenerator length, m
N	Speed, RPM
N_B	Beale Number
N_c	Number of cooler tubes
N_e	Number of heater tubes
P	Power, W
p	Pressure, kg/m^2
P_{fr}	Frictional power, W
p_{ref}	Operating pressure, kg/m^2
Q_{in}	Heat input, W
R	Gas constant, kJ/kg-K
t	time, s
T	Temperature, K
T_C	Sink Temperature, K
T_H	Source Temperature, K
v	velocity, m/s
V	Volume, m^3
V_{sw}	Swept volume of the engine, m^3
α	Thermal diffusivity, m^2/s
γ	Heat capacity ratio
δ_r	regenerator mesh wire diameter, m
η	Efficiency, $\%$
μ_0	Dynamic Viscosity at 300K, N-s/m^2
ρ_w	Density of regenerator material, kg/m^3
τ	Ratio of convective to diffusive heat transfer time scale
ϕ	Porosity

CHAPTER 1

Introduction

Decentralized power systems using renewable sources like biomass and solar are attractive options to meet the energy demands (power, heating and cooling) in areas with limited or no access to grid. Available technological solutions include biomass gasification and solar PV. Of the thermal energy based systems, biomass gasification is the most common. Using the well known IISc biomass gasification technology, over 40 installations with single units up to a few 100 kW_e and multiple units up to a combined capacity of a few MW_e have been implemented across various parts of India and abroad for applications ranging from industrial captive power and rural electrification to thermal requirements. An overview of this technology can be found in Mukunda (2003). It is clear from Mukunda (2003) that while the technology is mature enough for large scale implementation, issues related to biomass supply chain need further attention to ensure sustained high plant load factors and hence overall economy.

On the other hand, almost half of the world's population use some form of biomass in traditional devices for cooking and heating. Efforts to improve this scenario has also led to the recognition of the potential of domestic power generation systems. The perceived advantage being the simplicity of coupling this to heating needs, which is mostly cooking in India. Given that still significant fraction ($\sim$ 80%) of rural Indian households use some form of traditional fuels (firewood, cow dung etc.,) in traditional chulas at very low thermal efficiency (10-15%) to meet cooking energy needs, there is large potential for dissemination of improved devices to reduce fuel consumption and emissions. A significant fraction of this population also lacks access to electricity (estimated at 225 million as of 2013 in Birol (2015)). This has led to the exploration of combined power generation of a few 100 W to meet the lighting and other power needs of off-grid rural households. Promising candidate technologies include Stirling engines and thermoelectric-generators (TEGs).

Of these, TEGs have received increasing attention in the past two decades. With no moving parts, TEGs are the simplest of the candidate technologies. A number of studies on development and optimization of TEG based domestic power generation systems coupled to cooking devices can be found in literature (see, for instance, Champier *et al.* (2011); Lertsatitthanakorn (2007); Mastbergen (2008); Nuwayhid *et al.* (2003)). In all these studies, commercially available TEG modules are integrated with an improved cooking device to generate power with an overall efficiency of 2-5%; in this respect, TEGs are very similar to solar PV modules, in that the efforts are directed towards overcoming problems related to integration and downstream systems. Hence any significant cost cutting depends on the cost and efficiency of the modules itself. In the light of this situation there is still scope for exploration of alternate options for small scale power generation. One such option is based on *Stirling engines* with a distinct advantage of reasonable efficiencies ($\sim$ 10-20%) at low power (few 100 W electricity) using external combustion and hence fuel flexibility and lesser emissions as compared to IC engines in this power range.

1.1 Stirling engine

The term 'Stirling engine' usually refers to a class of external combustion closed cycle 'air engines' (including engines using other gases as working fluids). Stirling engines have been used in specialized applications like cryo-coolers and power generation in space (the STC 55 W free piston engine for example), where reliability and performance (typically 20-40 % efficiency) are most important with little or no attention to cost per kW. As pointed out in Mastbergen (2008), for waste heat applications a lower efficiency could be tolerated if the cost is sufficiently low - this is considered a very challenging problem. A few developmental efforts have focused on cost effective Stirling engines - these efforts can be grouped into three categories based on power output, namely, high (>10 kW class), medium (1-10 kW class) and low/domestic (few tens to few hundred W class). The NASA P40 engine capable of generating 41 kW at 27.5% efficiency (Kelm *et al.* (1981); Ernst and Shaltens (1997)) and a 4 cylinder hermetically sealed 40 kW engine with 37.5% efficiency using wood chips as fuel by Carlsen and group from Denmark (see Carlsen *et al.* (1996)) are two examples belonging to the high power category. The 3 kW engines reported in Lane *et al.* (1989); Thorsen *et al.* (1996); Kagawa (2000); Takizawa *et al.* (2004) belong to the medium power category. Both high and medium power ranges are such that these overlap with output range suitable for IC engine technology and hence the need for such engines is not clear. Details of a few domestic class engines in the output range of 50-600 W are shown in Table 1.1. Many small engines, mostly belonging to *enthusiast class* deliver negligible power at close to zero efficiency and are not discussed here (Kongtragool and Wongwises (2007) for instance).

Table 1.1: Domestic power range engines

Source	Engine type	Working medium	Power (W)	Pressure (atm)	Source Temp (°C)	Efficiency (%)
Hirata *et al.* (1997)	γ	Helium	100	8	650	-
Karabulut *et al.* (2000)	α	Air	65	2.5	1100	-
Hoshino *et al.* (2000)	γ	Helium	585	30	600	32
Cinar and Karabulut (2005)	γ	Helium	128	4	700	-
Batmaz and Üstün (2008)	α	Helium	118	1	1000	11
Karabulut *et al.* (2009)	β	Air	51	2.8	200	15
Gheith *et al.* (2012)	γ	Air	500	8	550	35
Cheng *et al.* (2013)	β	Helium	390	8	850	32
Duan *et al.* (2015)	β	Air	289	15	600	-

The 200 years history of Stirling engine development has been checkered with periodic surge of activity followed by long dormant times. The mere mention of Stirling engine evokes one of the following extreme responses - either one of enthusiasm at the fact that there is still interest in the idea perceived to have enormous potential or skepticism that it is highly unlikely for any workable technological solution to emerge given that it has not happened over 200 years of considerable effort. This situation is partly due to the large presence of '*enthusiasts*' contributing a variety of working engine designs without necessarily being aimed at any relevant application and hence very little attention to performance and parameters affecting it. This is somewhat similar to the improved cook stove scenario, where a variety of designs are talked about without any reference to fundamental combustion parameters (see Varunkumar (2012) for details).

1.2 Modeling and analysis of Stirling engines

Somewhat independent from engine development efforts, a number of attempts have been made to understand and analyze thermodynamic processes in the Stirling engines. Most efforts, particularly the earlier ones (Schmidt (1871)) seem motivated by the similarity of the basic Stirling cycle with that of Carnot. Methods of increasing complexity starting from lumped zeroth order analysis to nodal methods (higher order methods) employing simplified forms of conservation equations have been developed to understand the operation and performance of real Stirling engines (see, for instance, FINKELSTEIN (1960); Urieli and Berchowitz (1984); Carlson *et al.* (1990); Martaj *et al.* (2007); Timoumi *et al.* (2008); Snyman *et al.* (2008); Cheng and Yu (2010); Formosa and Despesse (2010); Karabulut (2011); Asnaghi *et al.* (2012); Tlili and SaâĂŹed (2013)). Losses are estimated either separately (de-coupled) or as a part of the solution of the equations employed. A review of the earlier methods can be found in Martini (1978) and a more recent review of low temperature engines can be found in Kongtragool and Wongwises (2007). Most efforts, through parametric variation, estimate the influence on engine performance and in a few cases the results are compared with experiments; for instance Timoumi *et al.* (2008); Snyman *et al.* (2008) use the experimental results of GPU-3 engine and Asnaghi *et al.* (2012) use that of SOLO 161 solar engine. It is to be noted that the results of the models cannot be taken as predictions as they are obtained through parametric studies. Similar studies focused on obtaining desirable heat exchanger characteristics for engines have also been performed (see Thombare and Verma (2008)). Work of Prieto and group (see Prieto *et al.* (1994, 2000)), Iwamoto *et al.* (2001) and Organ (2013) can be considered an improvement over the other methods as they employ dimensional analysis coupled with thermodynamic models. This has led to an improved experimental correlation of indicated power with Beale/West number (which, as shown later is related directly to the mean effective pressure) and other engine geometric and kinematic parameters. Experimental results from select engines is subject to regression analysis for estimating correlation constants. The conclusions drawn are limited by the experimental data set to a large extent and hence lack generality. But the takeaway is that the increasing complexity of the models points in the direction of CFD simulations for parameter free predictions leading to a reliable design tool.

1.2.1 CFD studies

Last two decades has seen increasing number of CFD analysis of Stirling engines. Noteworthy amongst these is the 'Stirling 3-D simulation program' at NASA Glen Research Center. Detailed description of the efforts can be found in Zhang and Ibrahim (2004); Ibrahim *et al.* (2004); Dyson *et al.* (2005*a*,*b*, 2008). Apart from some preliminary validation studies, the current status of these efforts are not known. One of the earliest

CFD study is due to Mahkamov (2006*a*) in which an axi-symmetric model of a solar V-type Stirling engine was simulated. The standard $k - \epsilon$ turbulence model, with a dynamic mesh to reflect the reciprocating motion of the piston was used to obtain the gas temperatures, pressure distributions, velocity fields and the PV diagram. The results were compared with that from second-order models. It is not clear as to how the use of $k - \epsilon$ model is justified without sufficient information to deduce the nature of flow in the tubes. Also the inclusion of effect of compressibility is not justified as the peak flow velocities are much smaller compared to the speed of sound. Studies due to Mahkamov (2006*b*); Chen *et al.* (2014); Salazar and Chen (2014) also suffer from similar shortcomings. Alfarawi *et al.* (2016) presented the development and validation of CFD model of 500 W γ-type engine prototype to highlight the effects of phase angle and dead volume variations on engine performance. They found that the optimal phase angle was 105° rather than the generally accepted 90°. Several studies have focused on individual components, especially regenerator (see Costa *et al.* (2015) for instance). Without results from integrated CFD analysis of the entire engine, the usefulness of such studies are difficult to assess.

1.3 Motivation and Current effort

None except the NASA Glen research center program (the status of which is not known currently) have focused on development of CFD based design tool. Lack of a unifying theoretical framework for understanding the performance of these engines is a major hurdle in developing new designs. While a number of attempts have been made in the analysis of a given engine design that can be found reported in literature they are of very little use to design and develop new engines. Notably, no attempt has been made to predict the performance of a variety of designs without adjustable parameters. Current work aims at developing such a tool by employing a combination of CFD and dimensional analysis. It is not usually recognized that in addition to engine geometric-kinematic details and operating pressure and speed, precise data on external heat transfer processes are required for developing reliable simulation tools. Since this is not generally available in literature, a V-type air engine was designed and developed as a part of this work mainly for measuring external heat transfer parameters and frictional power. The CFD simulations make effective use of the experimental results along with dimensional analysis towards development of a design tool. An improved engine design procedure is an important outcome of the current work.

1.4 Objective and scope

The objective of the study is fundamental experimental and computational investigation on an α-type Stirling engine with the aim of developing a robust CFD based design tool. The scope of the investigation includes -

1. Development of a lab scale α-type Stirling engine for experimental studies on heat transfer and frictional characteristics.
2. Identify critical parameters using dimensional analysis.
3. Develop a 2D-axisymmetric CFD model to establish quantitative relationship between the non-dimensional parameters.

1.5 Thesis organization

The thesis is organized as follows -

1. Chapter 1 - Introduction
2. Chapter 2 - Experimental studies
3. Chapter 3 - Computational studies
4. Chapter 4 - Results and discussions
5. Chapter 5 - Conclusions and future work

CHAPTER 2

Experimental studies

In this chapter the details of the experimental studies are presented. The first part of this chapter describes the design of the experimental V-type engine along with details of instrumentation and the second part describes the hot and cold operating characteristics and frictional power measurements.

2.1 Engine design

A single stage two cylinder 2 hp air compressor was chosen as the initial configuration. The two cylinders have same dimensions with bore and stroke of 60 mm. The cylinders are arranged 100° apart. This arrangement allows the two pistons, that are connected to the same shaft through their respective connecting rods to reciprocate with a phase difference of 100°. A phase difference a little greater than 90° is required between the cylinders for one of those to function as compression side (cold) and the other as expansion side (hot). Therefore a compressor with 100° phase difference was chosen for the studies. The specifications of the configuration are given in Table 2.1.

The heads of the two cylinders and the valve mechanism were removed and replaced by heater, cooler, and regenerator. A separate cooling jacket for the expansion cylinder was also added so as to keep the aluminum piston from melting and over expansion. Photographs of the lab engine showing the front view and the side view are shown in Fig. 2.1.

2.1.1 Heater

The heater consists of 9 tubes with an average length of 260 mm and an internal diameter of 7.8 mm. The tubes are made of SS310 grade stainless steel. A shell made of the same material covers the heater tubes. The assembly is a 2-fluid single pass shell and

Table 2.1: Specification and operating condition of the experimental engine

Component	Parameter	Value
Mechanical drive system	Piston diameter	60 mm
	Piston stroke (S)	60 mm
	Crank length	120 mm
	Phase angle	100°
Heater heat exchanger	Number of heater tubes	9
	Average heat transfer length (L_e)	260 mm
	Diameter of each tube (d_e)	7.8 mm
Cooler heat exchanger	Number of cooler tubes	9
	Average heat transfer length (L_c)	260 mm
	Diameter of each tube (d_c)	7.8 mm
Regenerator	Length	50 mm
	Diameter	50.8 mm
	Porosity (ϕ)	0.86
	Mesh number	30 × 32
	Wire diameter(δ_r)	0.2 mm
Operating conditions	Working fluid	Air
	Mean pressue (p_{ref})	1 bar
	Combustion gas temperature (T_H)	900°C

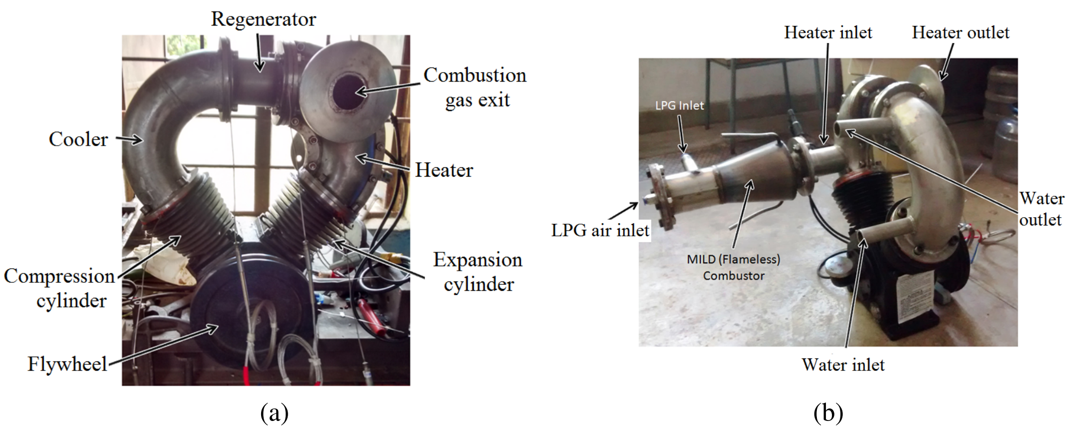

Figure 2.1: Photograph of the Lab Engine: (a) Front View (b) Side View

tube heat exchanger. Figure 2.2 shows heater heat exchanger of the prototype before assembly of the shell and tubes.

Figure 2.2: Heater tubes along with the shell before assembly

For the present purposes of studying heat transfer aspects it was decided to use a compact heat source. Towards this, an LPG based flameless combustion chamber with a nominal power of 6 kW$_{th}$ was designed. Flameless combustion is a preferred technique for designing compact heat sources with volumetric heat release rates upto 10 MW/m^3 (see Kumar *et al.* (2007)). Figure 2.3 shows the schematic of the 6 kW$_{th}$ flameless combustor. It consists of 4 inlet holes each of 0.6 mm and 2.5 mm for LPG and air respectively. The combustion chamber is made into a conical shape with a concentric cone inside to facilitate recirculation of the combustion products. Figure 2.4 shows the side view and top view of the combustion chamber in operation. The near transparent flame is characteristic of combustion under flameless (MILD) conditions.

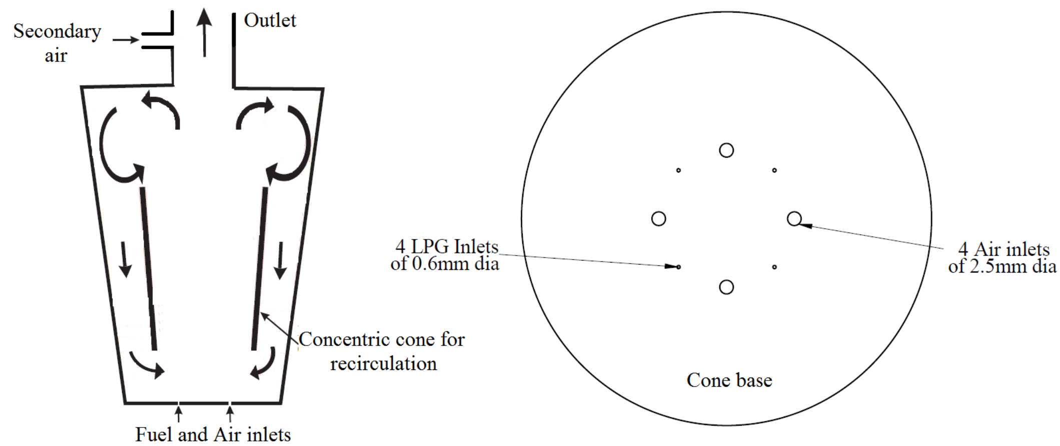

Figure 2.3: Schematic of the flameless combustion chamber

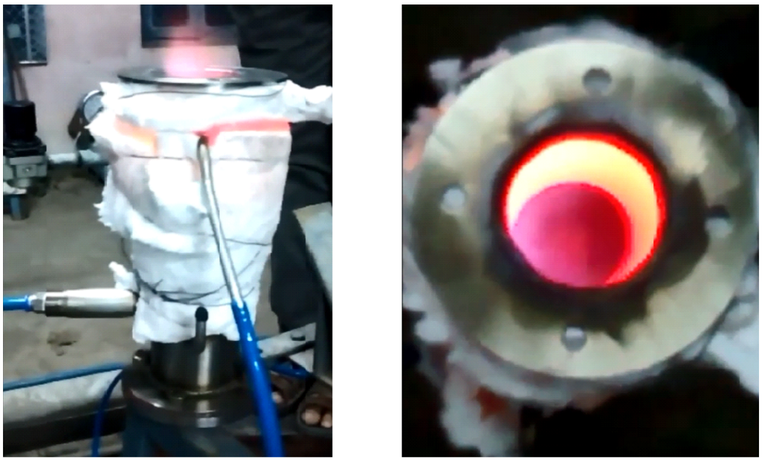

Figure 2.4: Side view and Top view of combustion chamber in operation

2.1.2 Regenerator design

The regenerator is the most important component of a Stirling engine. It is the heat exchanger in which the highest heat is transfered within a cycle in a given engine. This indicates that the engine performance of the engine depends greatly on the effectiveness and its ability to accommodate high heat fluxes (Urieli and Berchowitz (1984)). For this to be achieved, the thermal capacity ratio (TCR) must be greater than 10 (typically engines have values from 8 to 30 in the literature Organ (2013)). Thermal capacity ratio (TCR) is defined as the ratio of heat capacity of the matrix material to the heat capacity of the gas per pass at constant rate with uniform density. It is given by eq. 2.1.

$$TCR = N_{TCR}\left[\frac{\gamma - 1}{\gamma}\right]\delta_r\left[\frac{1-\phi}{\phi}\right] \tag{2.1}$$

where,

$$N_{TCR} = \frac{\rho_w c_w T_C}{p_{ref}} \tag{2.2}$$

and, γ is the ratio of specific heats, δ_r is the ratio of regenerator dead space to swept volume, ϕ is the porosity, ρ_w is density of the material, c_w is the thermal capacity of the material, T_C is the sink temperature and p_{ref} is the charge pressure. Organ (2013) recommends a TCR greater than 10 as a safe value for design of a regenerator. As TCR is a function of p_{ref} and the engine was intended to be tested at higher pressures as well, a high TCR of about 700 was chosen at p_{ref} = 1 atm. When the pressure is increased to 10 - 20 bar, the TCR reduces by 10 and 20 times respectively, bringing TCR to about 35. To choose the diameter of the wire in the mesh, the following scaling relation from

Organ (2013) is used:

$$d_w \sim \sqrt{\frac{\alpha}{N}} \tag{2.3}$$

where, α is the thermal diffusivity, and N is the speed of the engine in rpm. The relation shown in eq. 2.3 represents the fact that the time required for a single wire in the mesh to fully attain equilibrium with the gas temperature governs the diameter of the mesh wire. If the wire diameter d_w is too big, sufficient time will not be available for the heat to penetrate the center during a single blow (half cycle time). Thus some mass of the wire does not contribute to the storage of heat. If d_w is too small, heat penetrates to the center of the wire before the blow time expires. The square root of the ratio of the thermal diffusivity to one cycle timescale gives the depth of heat penetration in a cycle. Typical value of thermal diffusivity of stainless steel is 3.91×10^{-6} m^2/s. These values correspond to a wire diameter of around 0.1 mm from the eq. 2.3 for engine speed in the range of 100-1000 rpm. Given that this is an order of magnitude estimate, a stainless steel wire mesh with mesh number 30×32 (0.2 mm wire dia and 30 wires per inch) was chosen. A stack of 127 meshes was made. A photograph of the regenerator is shown in Fig. 2.5.

(a) (b)

Figure 2.5: Photograph of the regenerator: (a) Front view with the mesh (b) Side view

2.1.3 Cooler

Heater and cooler designs are similar and are geometrically symmetric about the regenerator. Cooler has 9 tubes made of Stainless steel SS310 with an average length of 260 mm and internal diameter of 7.8 mm. A shell made of the same material covers the cooler tubes. Water is used as a coolant.

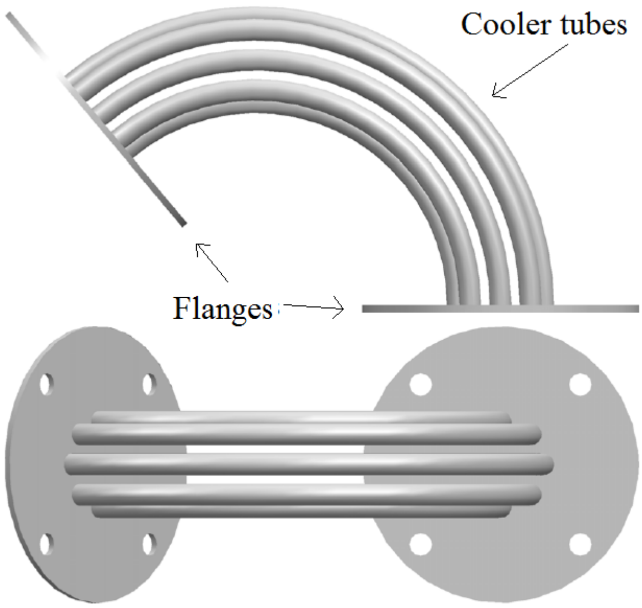

Figure 2.6: Front and top view of cooler tubes arrangement

2.1.4 Instrumentation

Temperature measurements

A K-type thermocouple of 1.5 mm bead diameter was introduced at the following places:

1. Between expansion chamber and heater
2. Between heater and regenerator
3. Between regenerator and cooler
4. Between cooler and compression space
5. At the inlet of the heater on the combustion gas side
6. At the outlet of the heater on the combustion gas side

Figure 2.7 shows the schematic of the engine showing the placement of various thermocouples.

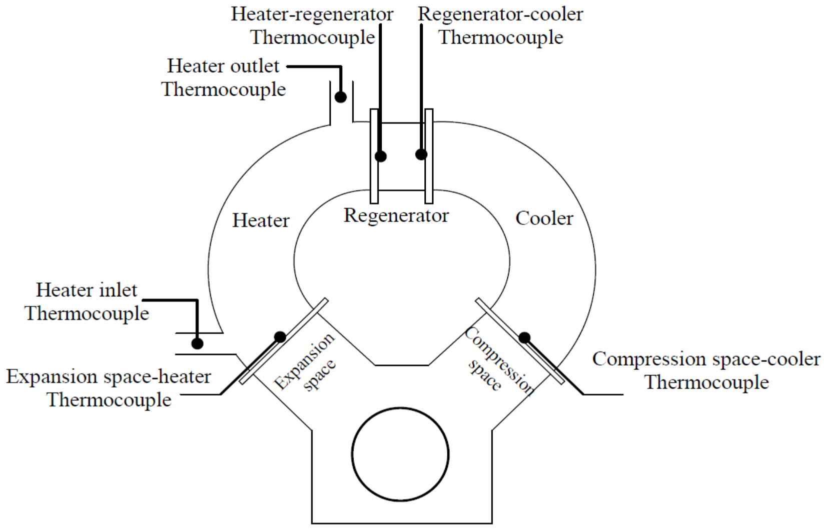

Figure 2.7: Schematic of the engine showing the placement of various thermocouples

These thermocouples were used at different stages of experimentation in the required combination. The thermocouples were interfaced to the Agilent 34970A/34972A data logger. Data was recorded by a computer connected to the Agilent data scanner and by using Benchlink Data Logger 3 software. The data is sampled at a rate of 1 Hz. Although the typical speeds of the engine is few hundred rpm and the cycle reverses direction every few milliseconds, the aim of the experiment is to estimate the average heat transfer coefficient for use in CFD calculations. Also preliminary CFD calculations revealed that the dominant resistance to heat transfer is due to the outer surface heat transfer coefficient and not from the unsteady flow on the working fluid side. Hence the oscillating heat transfer to the working fluid is due mainly to the changing temperature difference (ΔT) and not due to variation in the heat transfer coefficient of the internal surface (working fluid side). Therefore the 1 Hz acquisition rate was found sufficient. Also cylinder pressure measurements were not performed as a part of this study.

Flow measurement

IE rotameters were used to measure the volume flow rate of air and LPG to the combustion chamber. The rotameters have an accuracy of $\pm 2\%$ of the full scale reading. The range of rotameters used were 195 lpm for air and 22 lpm for LPG.

Tachometer

Figure 2.8: An EQ-801B Digital Tachometer

A LASER and contact type digital tachometer, EQ-801B, was used to measure the speed of the motor and the engine. The tachometer has resolution of 0.1 rpm for a range of 2.5 to 1000 rpm and 1 rpm for measurements beyond 1000 rpm and an accuracy of ±0.05 % of full scale. The tachometer has a sampling time of 0.8 s.

Electrical power measurement

CENTER 120 122 Digital multimeter was used to measure the current through and voltage across the DC motor used to crank the engine. The multimeter has a sampling rate of 2 Hz. It measure the DC voltage with an accuracy of ±(0.3%rdg+2dgt) and the DC current with an accuracy of ±(0.8%rdg+2dgt).

Figure 2.9: A CENTER 120 122 Digital multimeter

2.2 Motoring studies

A flywheel-clutch mechanism connected to a 1 hp DC motor assembly is used for cranking and motoring studies. The clutch system is a simple non friction positive type (dog) clutch which is used to disengage the motor pulley from the flywheel. Figure 2.10 shows the schematic of the engine crank case, flywheel and the clutch system mechanism. The engine must be stopped to re-engage the clutch. Figure 2.11 shows the complete assembly of the engine with the clutch system and the motor.

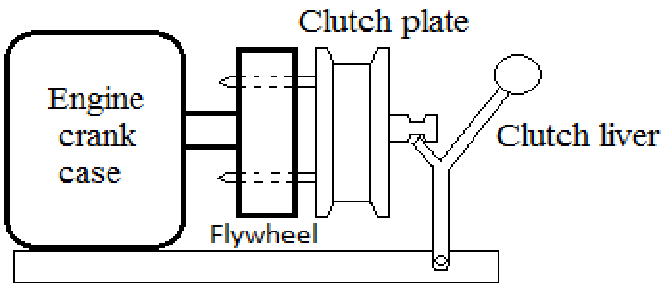

Figure 2.10: Schematic of the clutch assembly

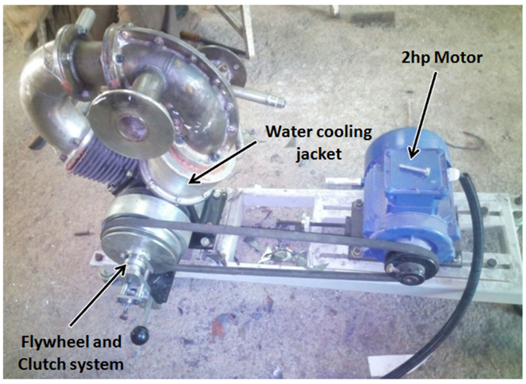

Figure 2.11: Complete assembly of the engine with the clutch system and motor

2.2.1 General operation

The engine was first run under cold condition i.e, without the combustion chamber running. The engine is cranked using a 1 hp DC motor through a pulley mechanism using a v-belt and a clutch system. The diameter ratio of the pulley is 1.83. The engine is supposed to run as a refrigerator, taking heat from (cooling) one of the heat exchangers and rejecting heat (heating) at the other, under this condition. A temperature gradient across the regenerator is to be observed. It was first thought that the position of heater and cooler is independent of the direction of rotation of the crankshaft, since the engine is geometrically symmetrical about the regenerator. But the experiments showed consistently that the temperature gradient flips its direction across the regenerator when the direction of rotation of the crank is reversed. The same was observed in the preliminary computational studies. Hence the direction of rotation is very important and the engine cannot run both ways once the heater and cooler are fixed. This happens due to the asymmetry in the thermodynamic compression and expansion of the gas because of the phase difference between the two pistons. The gas is compressed on one side of the regenerator (side where the piston leads) then displaced to the other side by a constant volume process and then expanded on the other side. Once expansion is done, the gas is again displaced at constant volume to the compression side. Therefore the compression always happens on the same side and expansion on the other side causing a temperature gradient across the regenerator when the direction of rotation is fixed.

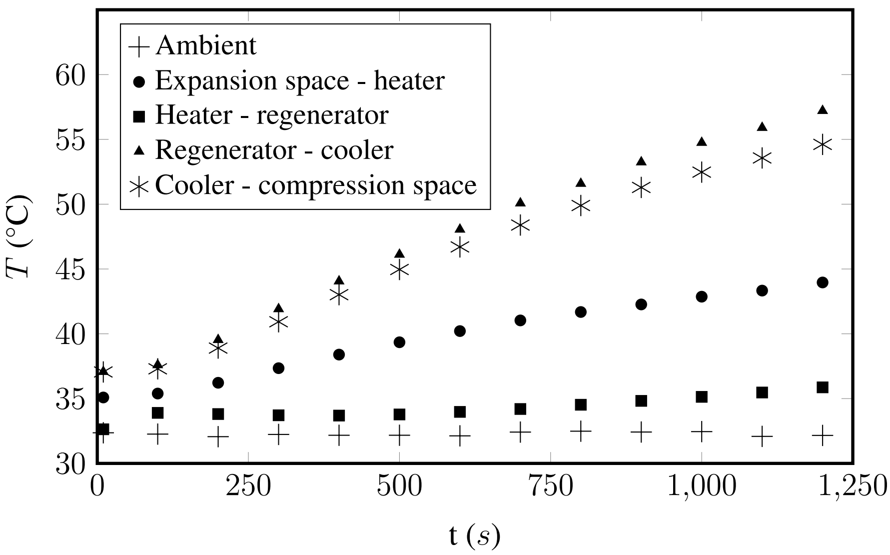

Figure 2.12: Transient establishment of temperature at different junctions of components

Figure 2.12 shows the transient establishment of a temperature gradient across the regenerator as the engine is cranked. Initially all the thermocouples read 32°C (not shown in the figure as the readings were taken after some preliminary run). When the cranking starts, the temperature between the regenerator-cooler starts increasing, while the temperature between the regenerator-heater reduces due to refrigeration effect (is almost constant in this case). This shows that the temperature gradient is established across the regenerator. The experiment shows that the regenerator plays a vital role in the stirling engine since in its absence, the temperature in the whole system would increase uniformly everywhere as adiabatic compression happens due to cranking in either direction. It also shows that the regenerator is quite effective at maintaining a temperature gradient.

2.2.2 Frictional power measurement

To design the engine it is important to determine the minimum power requirement which is determined by the losses due to friction. In order to measure the frictional power, the regenerator is first disassembled so that no power is consumed by the compression of the working fluid. The engine is run at constant atmospheric pressure. A 1 hp DC motor is used to crank the engine through a clutch assembly. The current through and the voltage across the motor are measured at various speeds. First the motor characteristics was measured. Then the clutch was cranked with the engine disengaged and its characteristics was measured. And lastly the engine characteristics with clutch engaged was measured. Figure 2.13 shows the measured values of current and voltage across the motor for full engine assembly. The product of the current and voltage at a particular speed gives the power consumed by the motor which is in turn the frictional power of the engine. The electrical efficiency of the motor is assumed to be close to 100%. Figure 2.14 shows the power consumed by the motor with speed for these three cases.

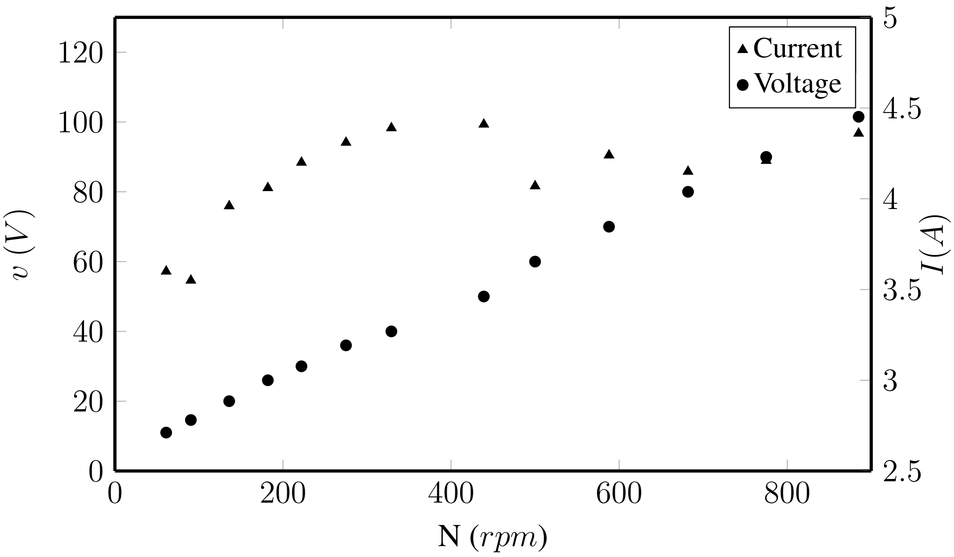

Figure 2.13: Experimental values of Current and voltage across the motor for various speeds

The power consumed by the motor and the clutch is subtracted from the full engine characteristics to get the engine frictional power with respect to speed. This is done by fitting linear regression lines to the data since measurement of power at exact speeds was not possible. Figure 2.15 shows the power characteristics of just the engine with respect to speed.

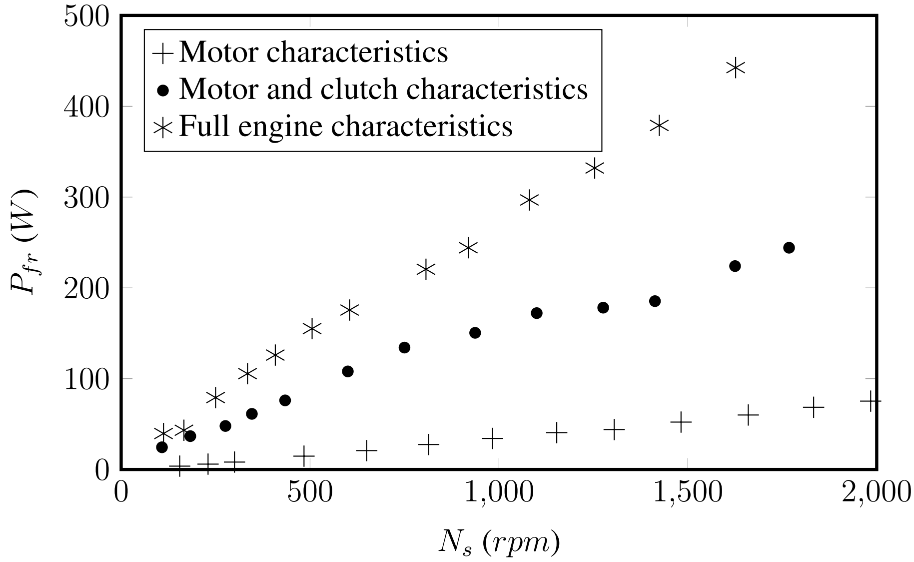

Figure 2.14: Frictional characteristics of various components with respect to speed

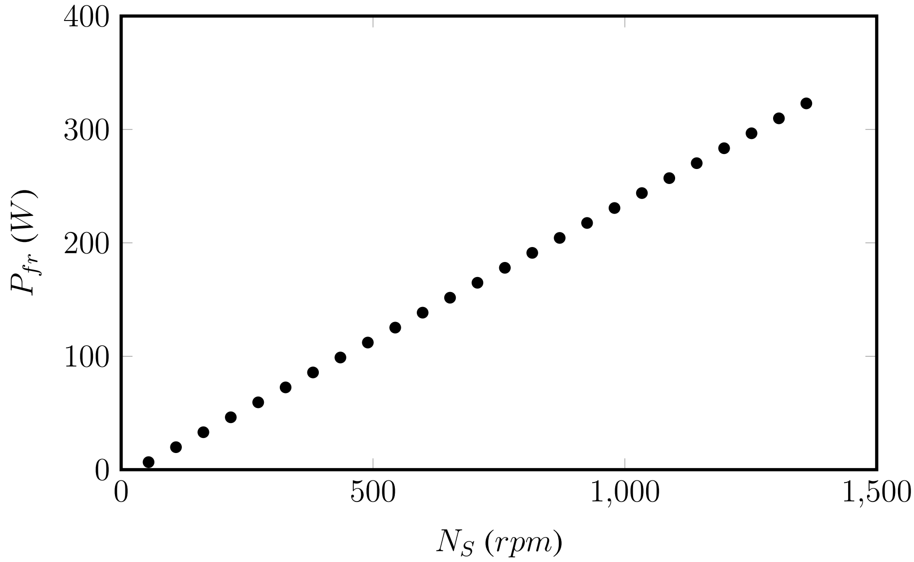

Figure 2.15: Frictional characteristics of the engine with respect to speed

2.2.3 Hot flow studies for heat transfer measurement

Preliminary computational studies suggested that although the efficiency of the engine was very good, the power produced by the engine was very low. This was attributed to the poor performance of the heater. It was found that the geometry (length and diameter) and the number of tubes plays an important role in the amount of heat that is added to the working fluid. Hence, measurement of the performance of the heater was critical.

A schematic of the experimental setup used for this is shown in Fig. 2.16. The

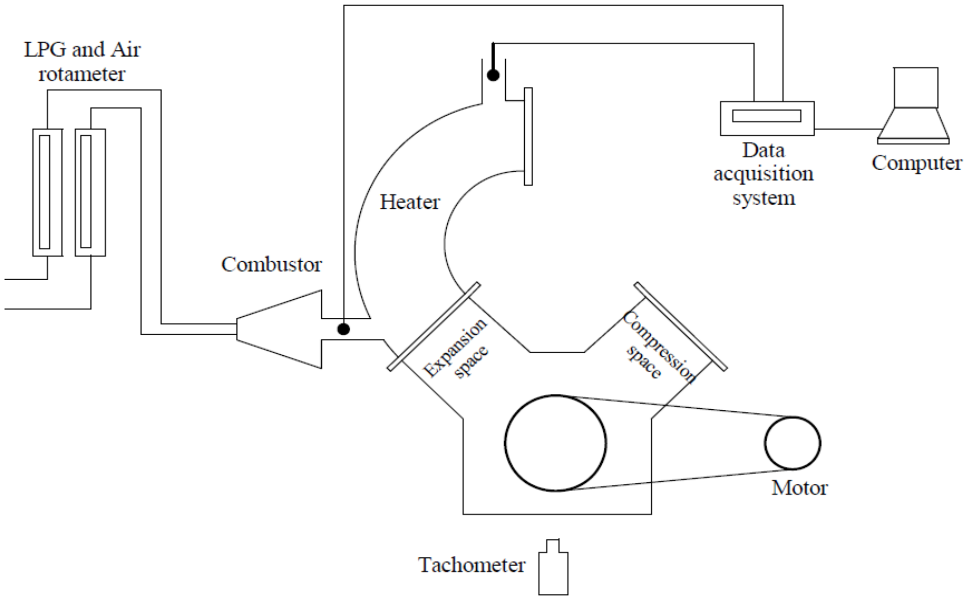

Figure 2.16: Schematic of the experimental setup

cooler and the regenerator were removed from the engine to study the performance of the heater alone. The flameless combustor was assembled with the heater. The combustor was run with a slightly lean mixture of LPG (2 lpm) and air (60 lpm) at 900°C. The temperature at the inlet and exit of the heater were measured at different speeds of the crankshaft. At each speed, the system is allowed to reach steady state (takes about 15 minutes) before the measurement. Figure 2.18 shows the thermocouple readings at the inlet and outlet of the heater. The expansion cylinder is cooled by the water in the cooling jacket so as to keep the aluminum piston from over-expansion.


Figure 2.17: Engine being cranked with only the heater assembled

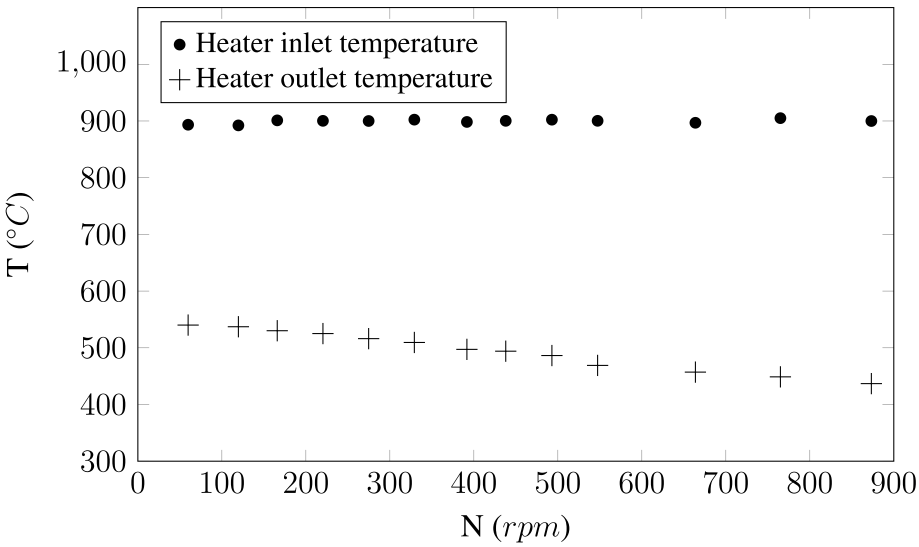

Figure 2.18: Experimental values of temperature at the inlet and outlet of the heater

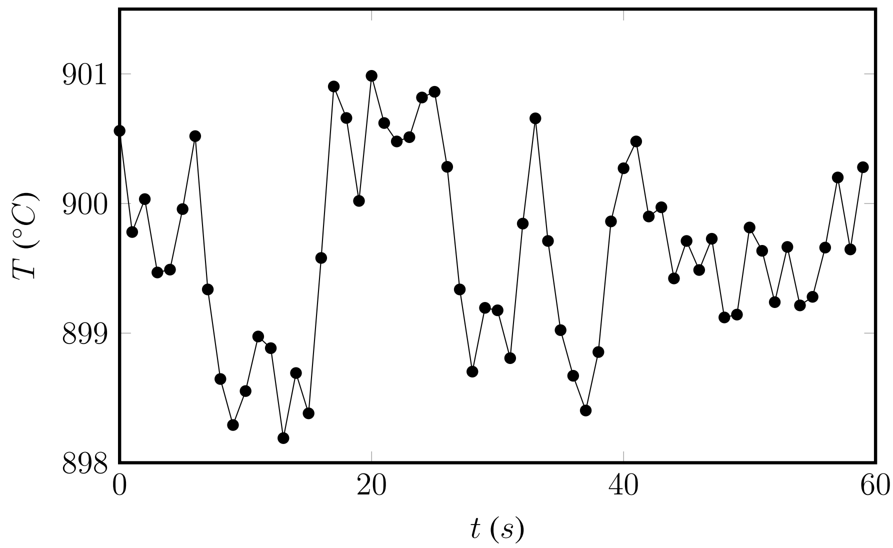

Figure 2.19: Temperature reading at the heater inlet for 60 s once the system reaches steady state

Experiment is started with stationary crankshaft. When the system reaches steady state, the temperature at the inlet and the exit of the heater are noted. Figures 2.19 and 2.20 show the temperature reading at the inlet and outlet respectively for 60 s once the system reaches steady state in a typical case. It can be seen that the temperature varies within ±5°C. The average of these values is taken as the final reading. Using the temperature difference between the inlet and the exit, the mass flow rate of the air and LPG, and a c_p value of 1.29 kJ/kg-K for the combustion gases, the amount of heat loss to the atmosphere is calculated. This value is subtracted from the subsequent readings made for different speeds of the crankshaft to give the heat transfer to the working fluid alone. Figure 2.21 shows the plot of the heat transfer from the combustion gases to

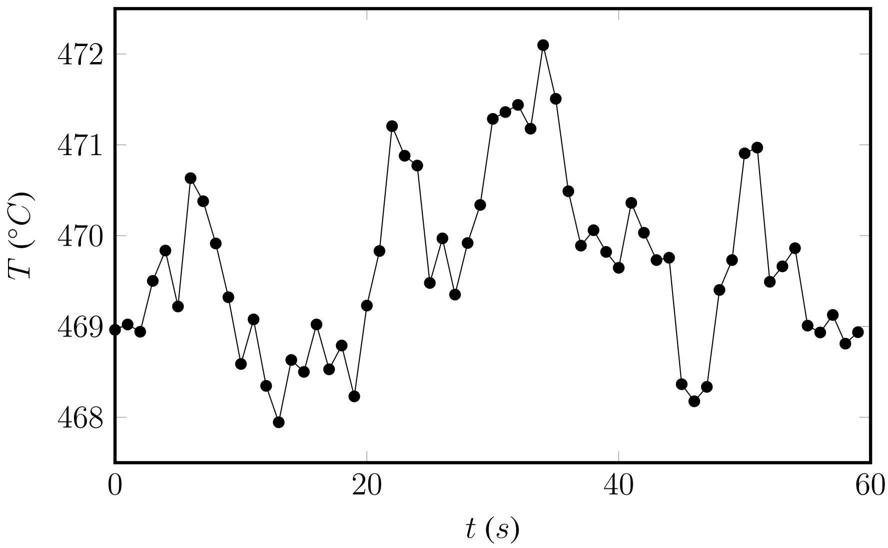

Figure 2.20: Temperature reading at the heater exit for 60 s once the system reaches steady state

the working fluid at various speeds. It can be seen that as the speed increases, the heat transfer increases linearly with a maximum heat transfer of 730 W at 873 rpm.

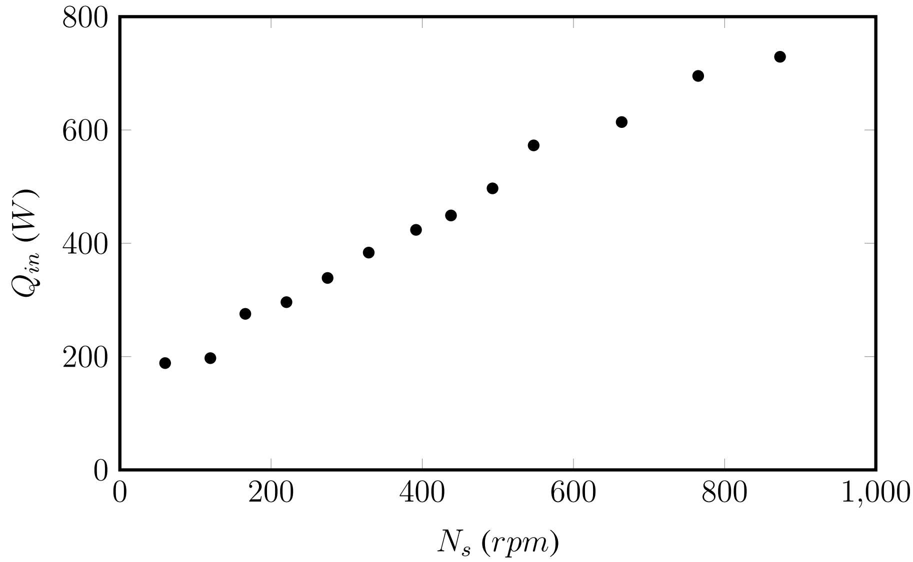

Figure 2.21: Heat transfer to the working fluid with respect to speed without the regenerator attached

These values are on the higher side since ambient air at 30°C enters the heater in each cycle. When the regenerator is attached to the heater, it is expected that the amount of heat transfer will significantly reduce due to the regeneration action. At steady state, the regenerator is expected to have a temperature gradient across it and the air entering the heater will not be at 30°C thereby reducing ΔT for the heat transfer.

2.2.4 Heat transfer measurement with regenerator

The regenerator consisting of a stack of 127 stainless steel mesh (mesh number 30×32) was assembled with the heater along with the cooler. Similar procedure as in the previous section was followed to obtain the heat transfer characteristics. Figure 2.22 shows the plot of heat transfer from the combustion gases to the working fluid at various speeds. As expected, it can be seen that the amount of heat transfer to the working fluid has significantly reduced due to the regeneration action. At 880 rpm the heat transfer to the working fluid is only 211 W as opposed to 730 W without the regenerator.

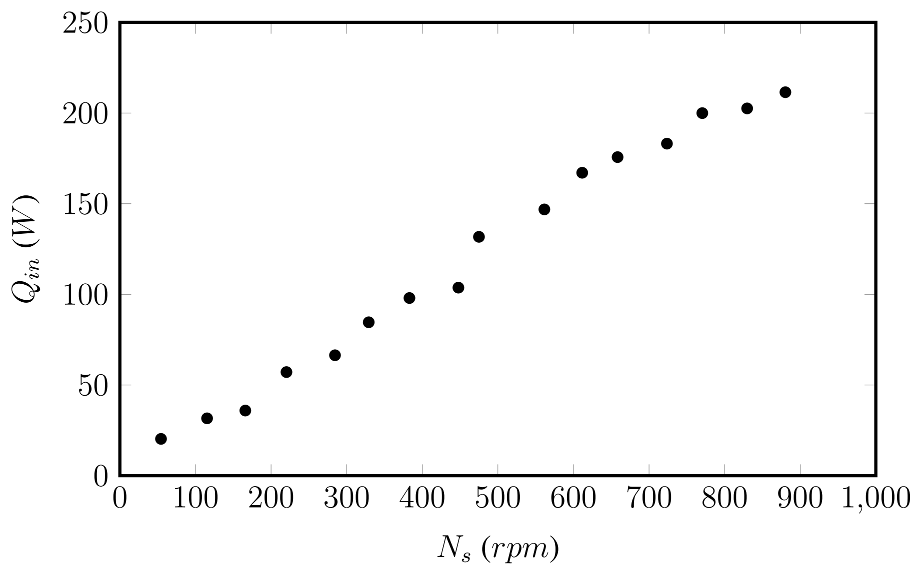

Figure 2.22: Heat transfer to the working fluid with respect to speed with the regenerator attached

2.3 Summary

An alpha type Stirling engine system has been designed and fabricated by modifying a single stage V compressor by addition of heater, cooler and regenerator. The following are the objectives of the experimental study

- Obtain heater characteristics
- Friction power measurements to determine the minimum required indicated power

Motoring and heat transfer studies showed that the frictional power loss was high compared to the amount of heat input to the working fluid through the heater. Hence the current design cannot produce useful work. But using the measured heat exchanger characteristics the performance of the current design was studied using CFD and dimensional analysis to identify the crucial parameters affecting the performance of the engine. Later the results are used to propose an improved design. The following chapter describes the dimensional analysis and the numerical computations carried out.

CHAPTER 3

Computational studies

In the first part of this chapter the dimensional analysis is outlined. The second part describes aspects related to computations, namely, the numerical model, boundary conditions, dynamic mesh modeling and grid independent studies. The cycle averaged results from the numerical simulation are presented.

3.1 Dimensional analysis

Twenty two variables - 12 geometric and 6 operating variables and 4 working fluid properties are identified as controlling parameters for the performance of the engine quantified by power output and efficiency. Table. 3.1 lists the variables. Expressing the engine power output (P) and efficiency (η) as a function of the identified variables as shown below, a Buckingham π analysis is performed to identify the geometric, kinematic and dynamics similarity groups.

$$P, \eta = f[V_{sw}, L_e, L_c, L_r, d_e, d_c, d_r, \delta_r, V_d, n_c, n_e, \phi, p_{ref}, T_e, T_c, N, h_e, h_c, R, c_p, \mu_0, k_0]$$

The geometric and kinematic similarity is largely dependent on the engine configuration and the choice of mechanism (slider-crack in α type). With heat transfer data available only for the experimental engine, the current study focuses on the dynamic similarity only, which is characterized by the non-dimensional group quantifying the ratio of the heat conduction time scale based on the heater tube diameter to the average piston speed based convective time scale denoted as, τ. An alternate method to arriving at the same dimensional group is discussed in the following paragraph.

Table 3.1: List of variable used in Buckingham's - Π analysis

Type of variable	Variable
Geometric	Swept volume (V_{sw})
	Heater length (L_e)
	Cooler length (L_c)
	Regenerator length (L_r)
	Heater diameter (d_e)
	Cooler diameter (d_c)
	Regenerator diameter (d_r)
	Mesh wire diameter (δ_r)
	Dead volume (V_d)
	Number of cooler tubes (n_c)
	Number of heater tubes (n_e)
	Regenerator porosity (ϕ)
Operating	Reference pressure (p_{ref})
	Source temperature (T_e)
	Sink temperature (T_c)
	Speed (N)
	External Heater heat transfer coefficient (h_e)
	External Cooler heat transfer coefficient (h_c)
Working fluid properties	Gas constant (R)
	Specific heat at constant pressure (c_p)
	Dynamic viscosity (μ_0)
	Thermal conductivity (k_0)
Performance	Power (P)
	Heat input (Q_{in})
	Heat output (Q_{out})

The time scale of heat transfer to the working fluid from the heat exchanger, that is, the conduction time scale is $t_{cond} = d^2/\alpha$, where d is the heater tube diameter and α is the thermal diffusivity of the working fluid. The time scale associated with the reciprocating motion of the working fluid caused by the piston, that is, the convective time scale is $t_{conv} = L_x/U_P$, where, L_x is the characteristic heater length and U_P is the average piston speed. The ratio of these two, designated, τ is given in eq. 3.1.

$$\tau = \frac{d^2 U_P}{\alpha L_x} = \left[\frac{p_{ref}}{RT_c}\right]\left[\frac{SNd_e}{30\mu_0}\right]\left[\frac{d_e}{L_e}\right] \tag{3.1}$$

where, the average piston speed $U_P = SN/30$, S being the stroke and N the engine speed in rpm. Prandtl number is assumed to be 1. Calculations were performed for τ ranging from close to 0 to about 30. As shown later, this single non-dimensional group is sufficient to capture the engine performance characteristics for a range of operating pressures, geometry and working medium.

3.2 Numerical model

In this study, a 2D axi-symmetric model of an alpha-type engine has been developed and simulated in ANSYS-Fluent. The aim of the CFD simulations is to establish a quantitative relationship between the identified dimensional group τ and principal engine performance parameters, namely, indicated efficiency and specific power. The simulation involves numerical solution of unsteady Navier-Stokes equation including the energy equation. Since the Mach number is always below 0.1, the flow is incompressible and the pressure based solver is used. The numerical model of the engine consists of a compression cylinder, cooler, regenerator, heater and expansion cylinder along the horizontal-axis in that sequence. The heater and cooler heat exchangers are modeled as axi-symmetric annuli. The hydraulic diameter D_h is given by $4A/P$, where A is the cross-sectional area and P is the perimeter of the cross section of tubes. The hydraulic diameter of the annulus is given by $D_h = D_o - D_i$. Using this equation the diameter, d, of the tubes is modeled as two times the width of the annular region. Figure 3.1 shows the axi-symmetric model of the base case corresponding to engine dimensions given in Table 2.1 at the initial condition corresponding to mean volume.

The following boundary conditions were used in the calculation.

- Convection boundary condition at 1000 K (average of the heater inlet and exit temperature) with 10 W/m^{2}K at the heater walls (chosen to match the measured heat transfer rate from experiments).
- Convection boundary condition at 300 K with 50 W/m^{2}K at the cooler walls

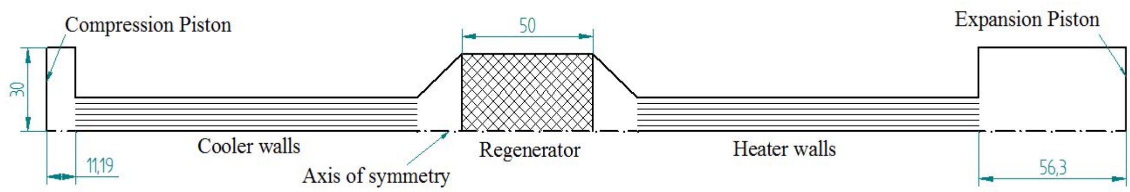

Figure 3.1: Axi-symmetric model of a typical case

- All other walls, including the pistons, are adiabatic
- The regenerator is modeled as porous medium with a porosity of 0.86 and permeability of 10^{-7} m^2
- Air, hydrogen and helium are used as the working fluid and are assumed to follow ideal gas law
- The operating pressure is varied from 1 bar to 10 bar
- The flow is unsteady laminar as the typical Reynolds numbers are well below 2000

A total of 72 simulations were performed by varying the heater and cooler lengths from 65 mm to 520 mm (65, 130, 260, 390 and 520 mm) so as to study the effect of variation in τ in the range of 0-30. The cylinder and piston dimensions were unaltered. The width of the annular gap is varied from 4 mm to 1 mm in steps of 1 mm. For a given length of the exchanger, the annular gap was varied keeping the volume of heat exchanger to within 2% of each other. Hence, the study was done for five different volumes and several surface areas representing several number of exchanger tubes. Three operating pressures, 1, 5 and 10 bar were used. The details are given in Table 4.1. Three different working fluids are used - air (R = 287 J/kgK, μ_0 =1.98$\times 10^{-5}$ Pa-s), helium (R = 2077 J/kgK, μ_0 = 1.96$\times 10^{-5}$ Pa-s) and hydrogen (R = 4124 J/kgK, μ_0 = 0.94$\times 10^{-5}$ Pa-s). The value of μ_0 for each of the gases is chosen at 300 K.

3.2.1 Dynamic mesh modeling

The reciprocating motion of the two pistons of the alpha Stirling engine are modeled as moving boundaries in the domain. The mesh is generated with the initial position of the pistons at the mean volume of the engine. An user defined function is written to give motion to pistons corresponding to that of slider crank mechanism (the udf code is given in Appendix A). The layers of cells are added or removed accordingly as the piston boundary moves. The addition and removal of cells adjacent to piston boundary is limited by maximum and minimum aspect ratio of 4 and 0.4 respectively. Different values ranging from 0.1 to 1 for minimum and 2 to 8 for maximum aspect ratios were tried out for different sizes of meshes. It was found that aspect ratios 0.4 and 4 were optimum for faster convergence. A time step equivalent to 1°, 5° and 10° were compared and it was found that time step equivalent to 10° rotation of the crank would give much faster solution without compromising on the accuracy of solution. A maximum of 150 inner iterations per time step. Typically the solutions converged in about 90 inner iterations. The simulations were performed for a physical time of 1200 s since the average physical time the computations took to arrive at steady values of variables was about 600 to 800 s.

3.2.2 Grid independence study

The geometry was meshed using GAMBIT 2.4.6. A grid independence study was carried out in order to check the sensitivity of the numerical results to the grid size. Three meshes were generated. One without prism layer to resolve boundary layer, and two others with near wall prism layer with first cell height 0.05 mm and 0.03 mm and growth ratio of 1.2. Figures 3.2 and 3.3 show the axial velocity profiles from the above three cases at one-fourth the length of the cooler from the compression space and heater from expansion space respectively at a time corresponding to 270° rotation of the crank. This condition at one-fourth length corresponds to peak velocity and gradients. It can be seen that all three cases agree closely with each other indicating grid independence.

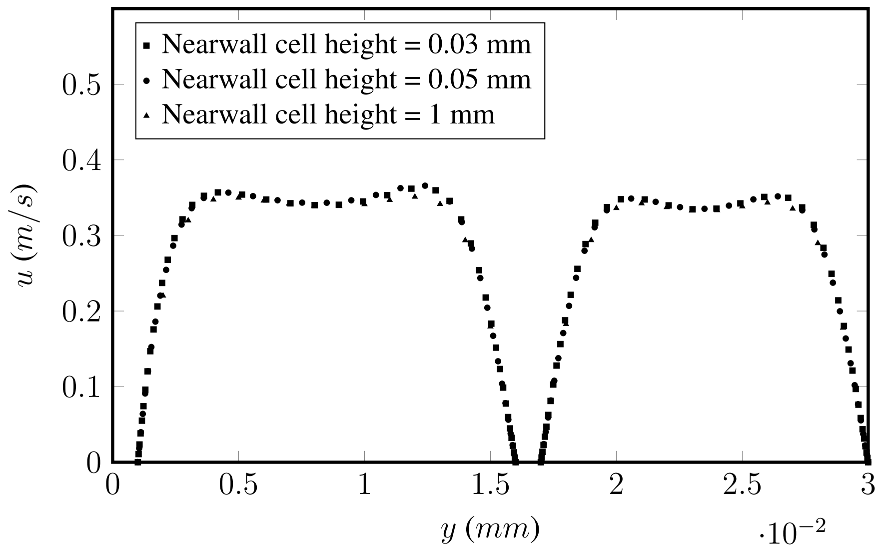

Figure 3.2: Axial velocity profile of a typical model at one-fourth the length of the cooler from the compression space

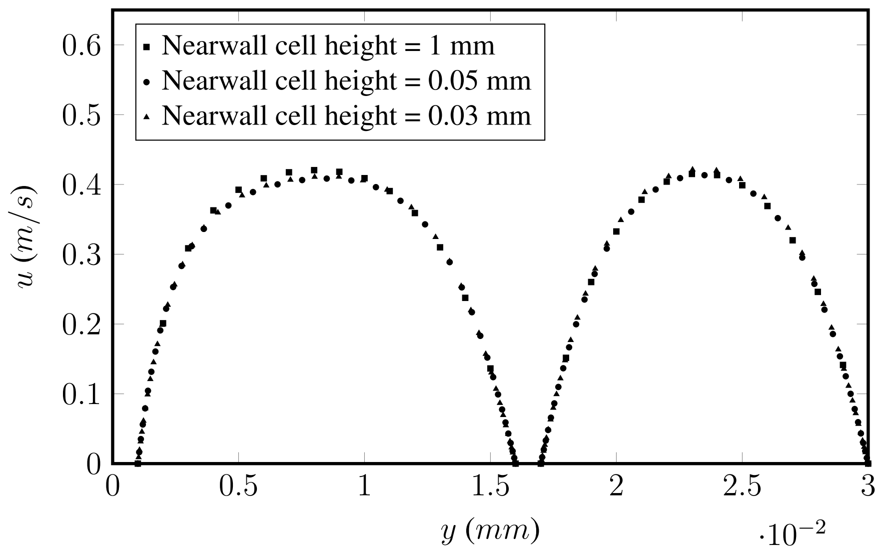

Figure 3.3: Axial velocity profile of a typical model at one-fourth the length of the heater from the expansion space

Simulations were performed using ANSYS-Fluent with the boundary conditions given above. The transient simulation is initialized with solution from steady simulation (that is, without piston motion). Figure 3.4 shows a temperature contour of a typical case after the steady calculation. Then a transient calculation was run with a time step equivalent to 10 ° increment in the rotation of the crankshaft for 1200 s for different engine speeds. Figure 3.5 shows the temperature contour after 1200 s. It can be seen that after 1200 s, a temperature gradient is established across the regenerator.

The cycle averaged pressure, temperature, heater heat flux and cooler heat flux ob-

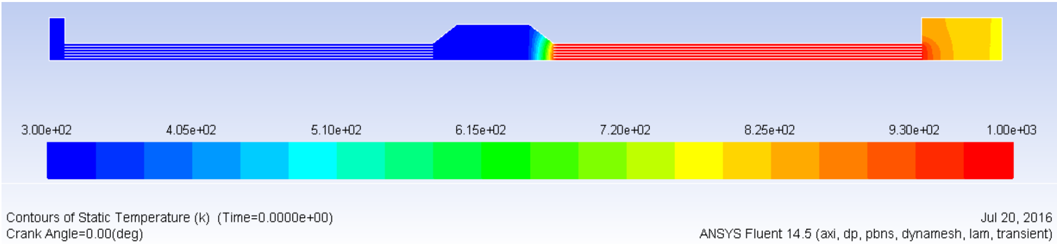

Figure 3.4: Temperature contour of a typical case after steady state calculation

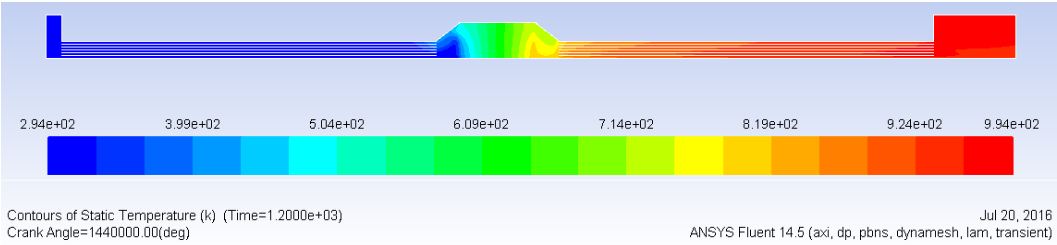

Figure 3.5: Temperature contour of a typical case after 1200 s

tained from the simulations are shown in Figs. 3.6, 3.7, 3.8 and 3.9. It can be seen that the cycle averaged values reach steady conditions beyond 500 s. The performance of the engine was evaluated using the flow variables once cycle averaged steady state is achieved. The heat input rate is calculated by taking the average heat flux over a cycle and multiplying it with the surface area of the heater.

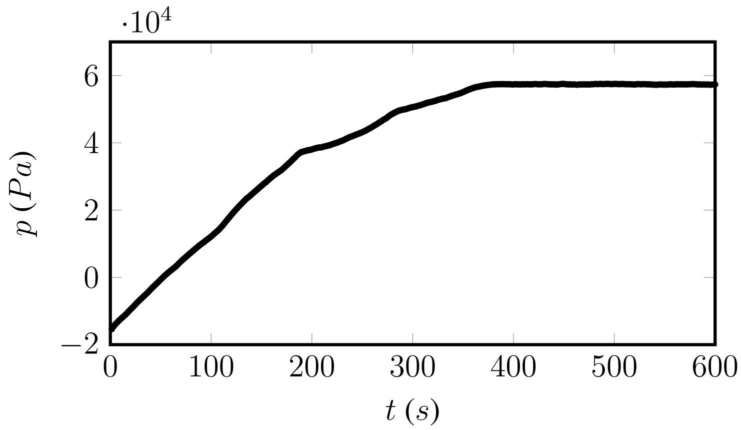

Figure 3.6: Average pressure (gauge) variation with time in a typical case

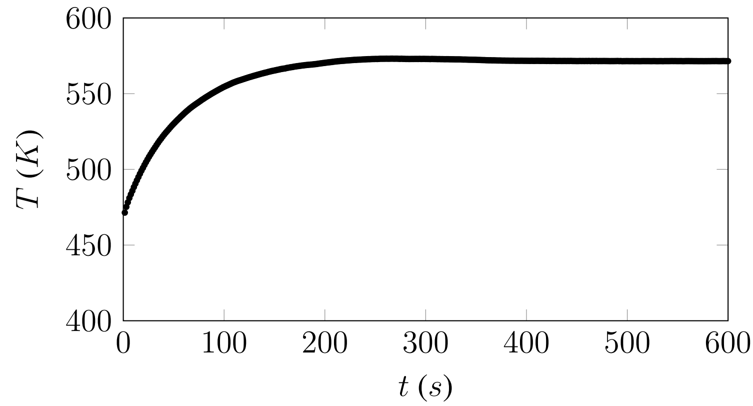

Figure 3.7: Average temperature variation with time in a typical case

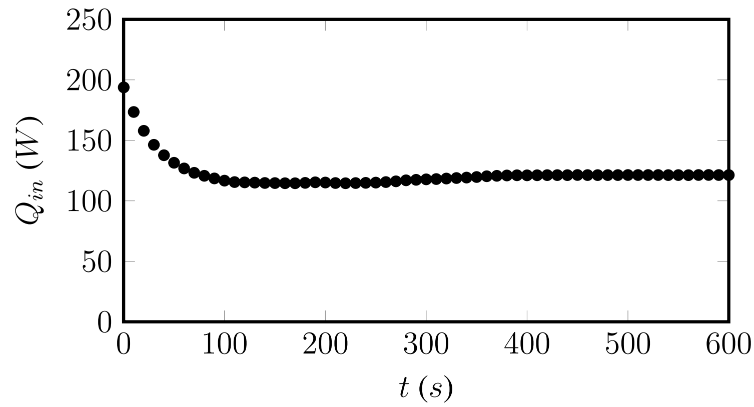

Figure 3.8: Heat input variation with time in a typical case

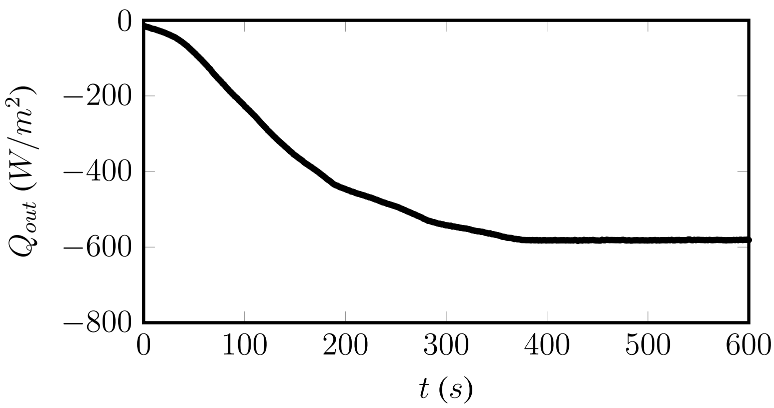

Figure 3.9: Average cooler flux variation with time in a typical case

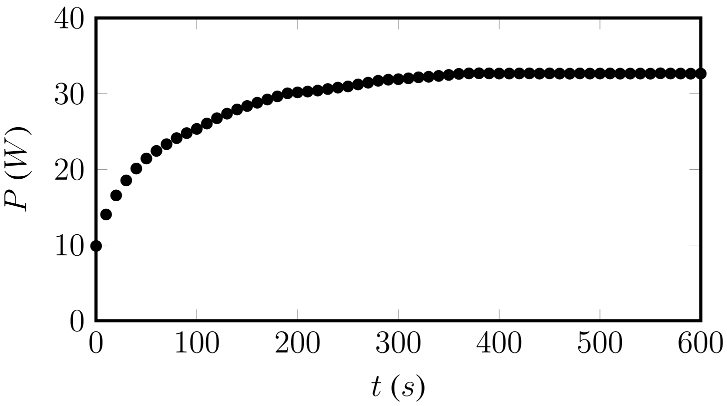

Figure 3.10: Variation of power with time in a typical case

3.3 Summary

A 2D axi-symmetric CFD model of an alpha type engine has been developed and simulated in ANSYS-Fluent. Grid independent study is done in order to check the sensitivity of the numerical results to the grid size. A non-dimensional number is identified to characterize the effect of the heater design on the performance of the engine. Results from the simulations are presented in the following chapter.

CHAPTER 4

Results and Discussions

In this chapter the results of CFD calculations are presented. Engine characteristics, namely, indicated efficiency and specific power variation for a range of geometries, speeds, operating pressures and working medium are shown to follow a universal function of the dimensional group τ derived in the previous chapter. Based on this feature an improved design procedure is set out.

In Table 4.1 the range of geometric and kinematic parameters along with different operating pressures and working medium used in the simulations are shown. Each one of these cases were simulated for a range of engine speeds (100 - 1000 rpm) and the corresponding values of τ is also shown. A total of 72 cases were simulated with τ varying from as low as 0.09 to as high as 32.

Some typical plots when the simulation reaches a steady state are shown in the following figures. Figures 4.1 and 4.2 show the variation of the total volume and pressure of the engine over a single cycle for the configuration C3 with heater tube diameter 6 mm and speed 400 rpm. Heat flux at heater and cooler over a cycle for the same case is shown in Fig. 4.3. Figure 4.4 shows the pV diagram of this case after it has reached steady state.

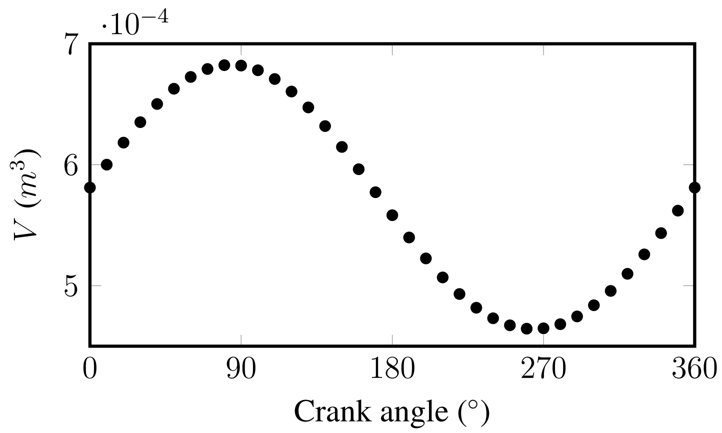

Figure 4.1: Variation of the total volume of the engine over a single cycle for the configuration C3 with heater tube diameter 6 mm and speed 400 rpm

Table 4.1: Parameter space explored with CFD

Configuration	L_e (mm)	d_e (mm)	p_{ref} (bar)	Working medium	τ
Base	260	7.8	1	Air	0.35 - 3.57
C1	130	6	1	Air	3.24 - 32.43
C2	130	4	1	Air	1.44 - 14.41
C3	260	6	1	Air	0.81 - 16.21
C4	260	4	1	Air	0.72 - 7.2
C5	390	8	1	Air	1.92 - 19.22
C6	390	6	1	Air	1.08 - 10.81
C7	390	4	1	Air	0.48 - 4.80
C8	390	2	1	Air	0.12 - 1.20
C9	520	2	1	Air	0.09
C10	260	4	5	Air	3.6 - 7.2
C11	260	2	5	Air	0.90 - 1.80
C12	390	4	5	Air	2.4 - 4.8
C13	390	2	5	Air	0.6 - 1.2
C14	260	4	10	Air	7.2 - 14.4
C15	260	2	10	Air	1.8 - 3.6
C16	390	4	10	Air	4.8 - 9.6
C17	390	2	10	Air	1.2 - 2.4
C18	520	2	10	Air	0.9
C19	130	8	1	Hydrogen	0.84
C20	130	6	1	Hydrogen	0.47 -0.95
C21	260	6	1	Hydrogen	0.23
C22	130	6	1	Helium	0.42 - 0.84
C23	130	8	1	Helium	1.5

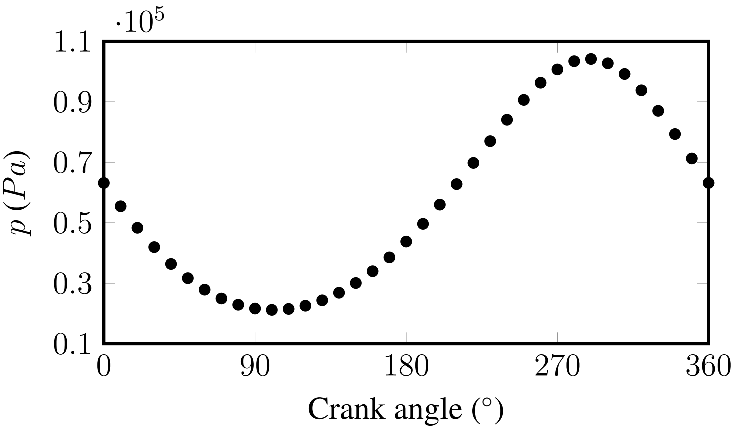

Figure 4.2: Variation of pressure(gauge) of the engine over a single cycle for the configuration C3 with heater tube diameter 6 mm and speed 400 rpm

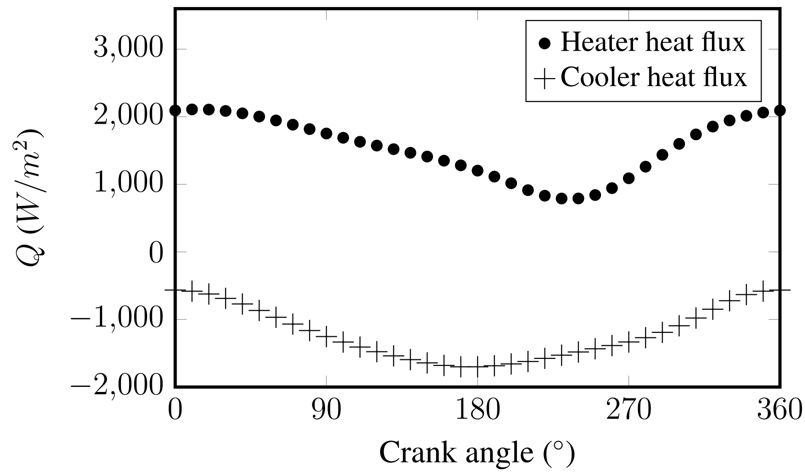

Figure 4.3: Heater and cooler heat flux of the engine over a single cycle for the configuration C3 with heater tube diameter 6 mm and speed 400 rpm

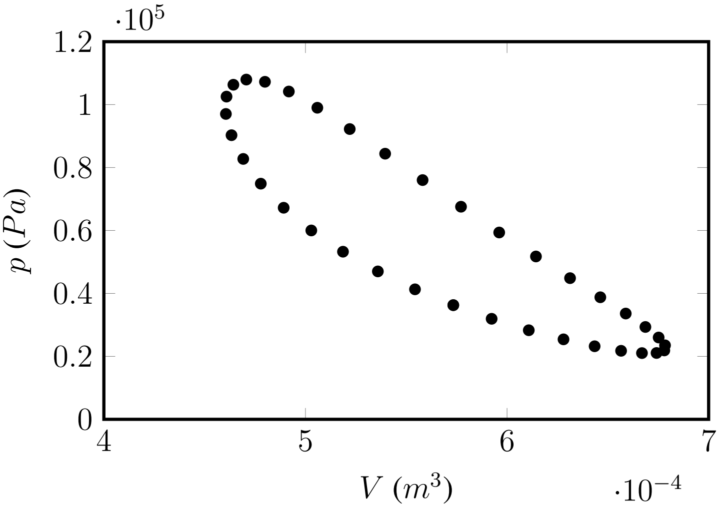

Figure 4.4: pV diagram over a single cycle for the configuration C3 with heater tube diameter 6 mm and speed 400 rpm

The importance of the non-dimensional group τ is brought out in the following figures. Figures 4.5, 4.6 4.7, 4.8, 4.9, 4.10 show the variation of pressure and heater heat flux and cooler heat flux in a single cycle for three different values of τ, namely, τ = 1.08 (case C6), 8.65 (case C6), 15.37(case C7). It can be seen that when the value of τ is near 1, the highest heater heat flux occurs near the highest pressure i.e, heat input and pressure are almost in phase (Fig.4.5). While for higher values of τ, the heat input and pressure are out of phase (Figs. 4.7 and 4.9). The same is true for cooler heat flux. When τ = 1, highest heat removal occurs when pressure is minimum (Fig. 4.6). And for higher values of τ, the heat removal is out of phase with pressure (Figs. 4.8 and 4.10). This is analogous to the Rayleigh criterion for amplification of pressure waves (sound) in a thermo-acoustic system. The results of the simulations indicate that for maximal conversion of random thermal energy to organized motion (work/pressure wave) the heat addition/removal must be broadly in phase with compression/rarefaction cycle.

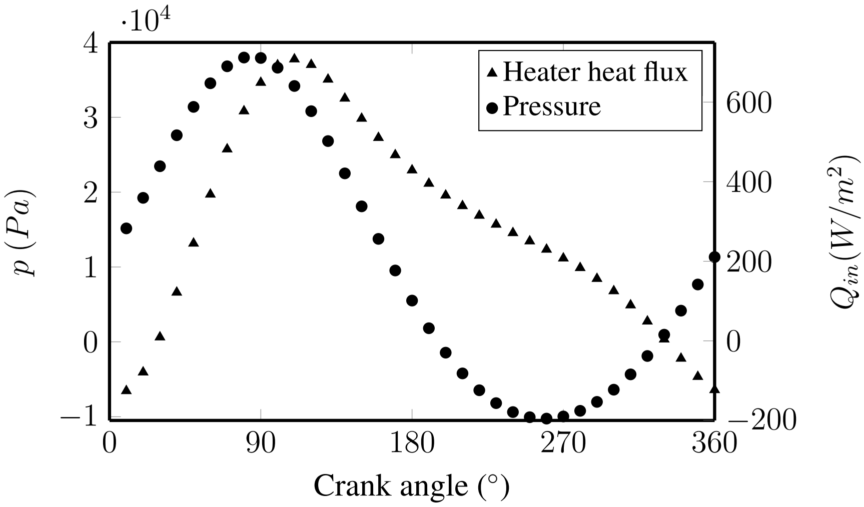

Figure 4.5: Variation of pressure(gauge) and heater heat flux with crank angle for $\tau = 1.08$ for case C6 (N=200 rpm)

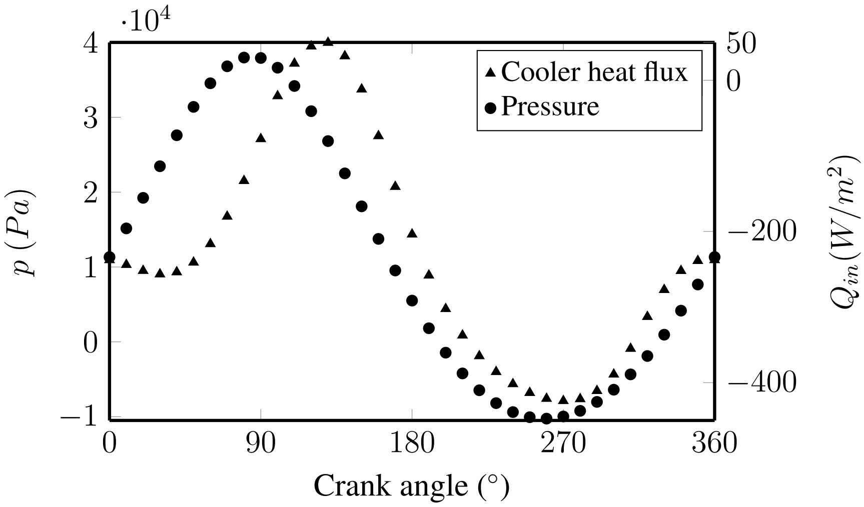

Figure 4.6: Variation of pressure(gauge) and cooler heat flux with crank angle for $\tau = 1.08$ for case C6 (N=200 rpm)

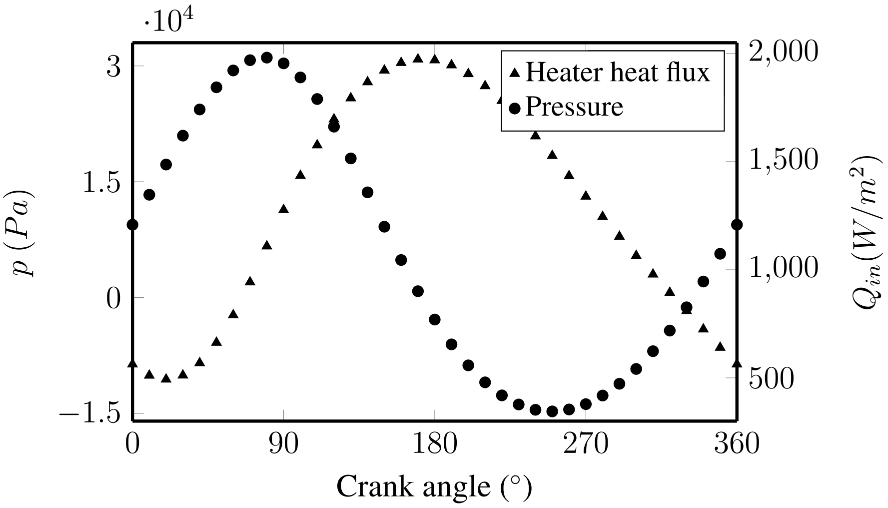

Figure 4.7: Variation of pressure (gauge) and heater heat flux with crank angle for $\tau = 8.65$ for case C6 (N=800 rpm)

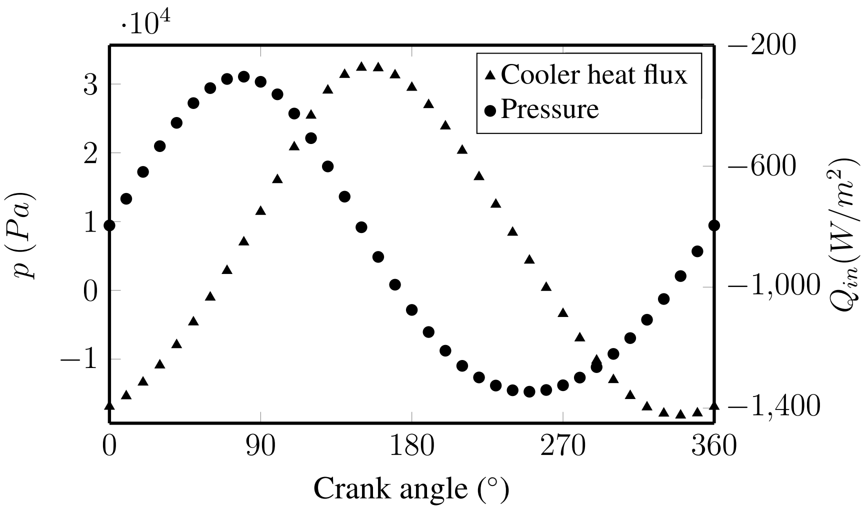

Figure 4.8: Variation of pressure(gauge) and cooler heat flux with crank angle for $\tau = 8.65$ for case C6 (N=800 rpm)

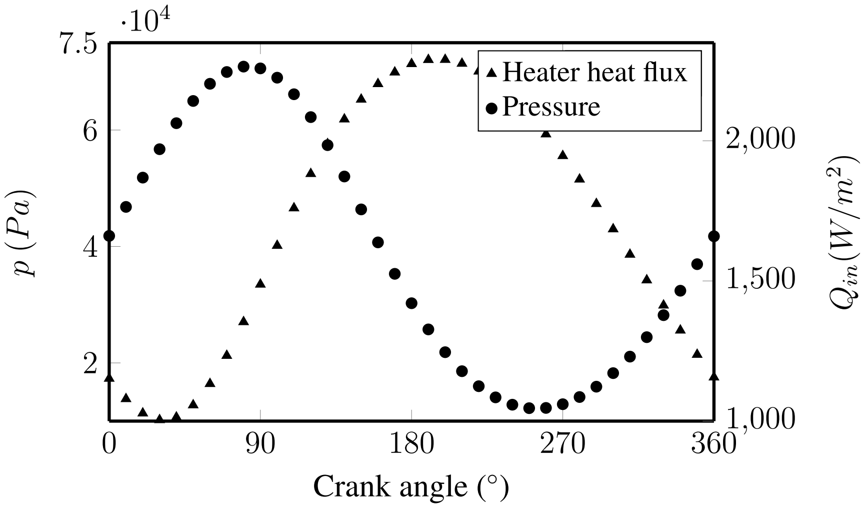

Figure 4.9: Variation of pressure (gauge) and heater heat flux with crank angle for $\tau = 15.37$ for case C7 (N=800 rpm)

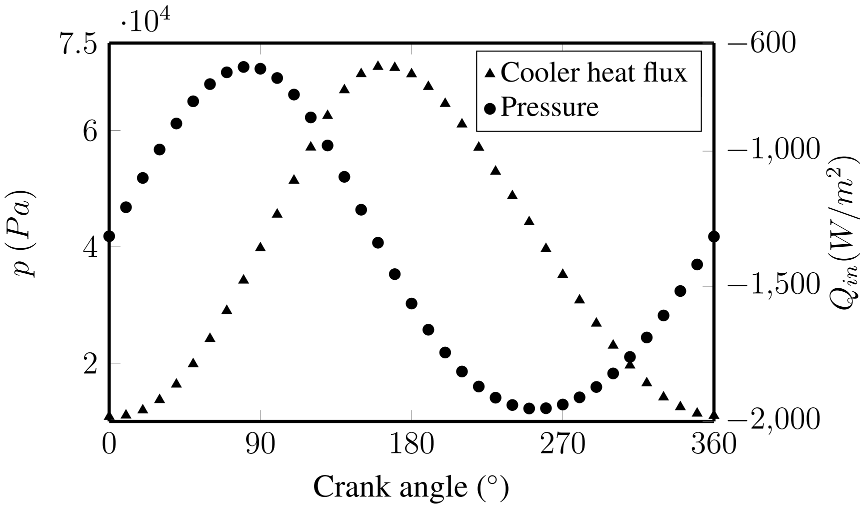

Figure 4.10: Variation of pressure (gauge) and cooler heat flux with crank angle for $\tau = 15.37$ for case C7 (N=800 rpm)

4.1 Characteristics of $\mathcal{T}$

Using the steady values of power output and heat input, the efficiency is calculated for each case and plotted against τ in Fig. 4.11.

The important observations are as follows -

1. All data, irrespective of the working fluid or operating pressure falls in a narrow band and follows similar trend.
2. The results clearly show a quadratic variation with very small efficiencies at very small and very high values of τ.

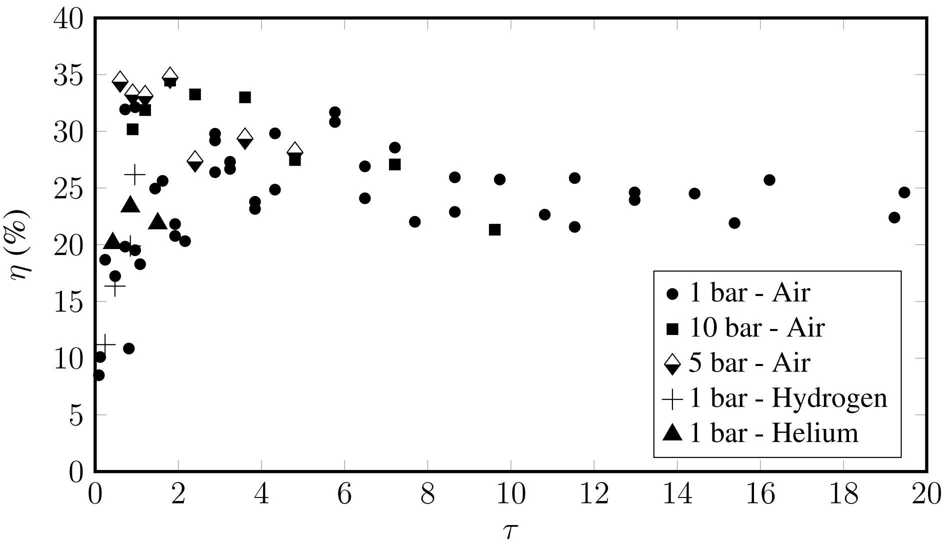

Figure 4.11: Indicated efficiency variation with τ

3. Efficiency increases as the value of τ increases and reaches a maximum at about τ = 1 and is almost constant until τ = 20. After this, efficiency reduces and goes to zero (not shown in the figure). This shows that there is a wide range of values of τ from about 0.5 to 20, which can be used to design heat exchanger for a given operating conditions, but preferably with τ = 1

It can be observed from Fig. 4.11 that higher pressures or change in working fluid lead to higher value of τ and therefore may lead to lower performance for a given external heat transfer conditions. This goes against the prediction of most models in the literature and generally accepted behavior of Stirling engines as they do not consider the effects of external heat transfer rate. An increase in pressure and/or change in working fluid cannot guarantee an improvement in performance unless corresponding changes in geometry and external heat transfer characteristics are made. This general feature of Stirling engines is clearly brought by the efficiency v/s τ plot.

The scatter in the plot can be attributed to the values of gas properties taken at reference temperature and pressure of 300 K and 1 bar respectively during the CFD calculations and other assumptions like Pr = 1 etc. The idea behind the plot is not to precisely predict the efficiency at any value of τ but only to help in the first approximation of the dimensions of the heater. The designer must keep in mind that the efficiency of the engine depends on many other factors such as regenerator effectiveness etc., and this plot is to be used for the back-of-the-envelop calculation for the heater design only.

4.2 Mean effective pressure

William Beale observed that the power output of Stirling engines confirmed approximately to the equation given in eq. 4.1 (Walker (1973)).

$$P = N_B p_{ref} V_{sw} N \tag{4.1}$$

where P is the Stirling engine power output, N_B is the Beale number, p_{ref} is the mean engine pressure in Pa, V_{sw} is swept volume in m^3 and N is the frequency of the engine in rps. He found that this relationship was approximately true for all engines in the literature including free piston engines. The combination $P/(p_{ref}NV_{sw})$ is called the Beale number which is a non dimensional group. The relationship shown is a gross approximation and there are examples in the literature that widely depart from the said value. The applicability of this simple relationship is clearly limited. Nevertheless, it provides a handy guideline for back-of-the-envelope calculations. Figure 4.12 shows the variation of N_B with τ obtained from simulation.

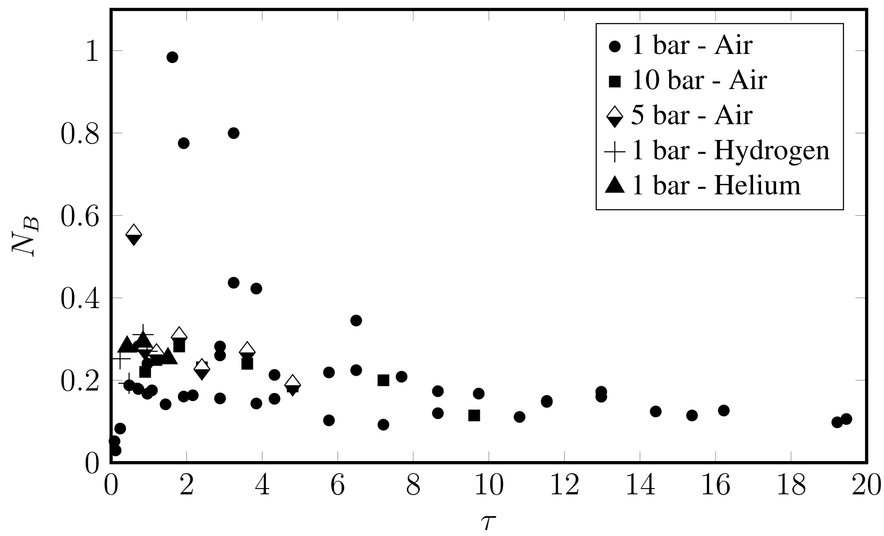

Figure 4.12: Characteristic values of N_B with respect to τ

It can be seen that the value of N_B calculated from CFD lies between 0.1 and 0.3 with most of the them having a value around 0.15, a feature common to many Stirling engines reported in literature. This indicates that the proposed CFD model is a reliable tool for prediction and design of Stirling engines unlike most other isothermal and adiabatic models proposed in the literature (see Walker (1973)). It is also an indication that the model is a more fundamental one that can be used over wide range of operating conditions and geometric configurations without the need for any experimental correlation constants.

Since the value of specific work (N_B) is almost always around 0.15, any need of higher power output demands higher rate of heat input to the working fluid which in turn demands increase in p_{ref} and/or speed of the engine, thereby increasing the value of τ. Correspondingly if the external heat transfer is not increased, the rate of heat input becomes drastically low compared to required power output. Therefore, an increase in the external heat transfer coefficient may not increase the efficiency at any given value of τ within the range stated above, but it would increase the range of τ within which the value of efficiency is acceptable. Therefore, the heat transfer coefficient on the combustion side plays an important role in the performance and design of the engine.

In the ideal Stirling cycle case, where the heat transfer coefficients on both sides are infinite (constant temperature heat input), the efficiency curve is a horizontal line at the Carnot's efficiency, which is dependent only the temperature ratio. The efficiency is independent of the pressure and speed and therefore independent of τ. But in the real cycle, performance reduces as the heat transfer coefficient on either sides reduces.

4.3 An improved engine design procedure

The following design sequence is proposed for domestic class (few tens to few hundred W class) Stirling engine.

1. Choose a convenient working fluid and speed N for a rated power P.
2. Apply specific power (Beale number) criterion to find the V_{sw} for a range of pressure that is acceptable for the application.

$$N_B = \left[\frac{P}{p_{ref} V_{sw} N_s}\right] = 0.15 \tag{4.2}$$

   As an example 200 W at 600 rpm is taken. Reference pressures of 1, 5 and 10 bar are taken as the range. Swept volume, V_{sw} (cc), will be 1330, 266 and 133 for the above three cases respectively. It is seen that, as the reference pressure is increased, the compactness of the engine increases as expected.
3. Choose a length L_e for the heater heat exchanger bearing in mind the considerations of fabrication, external heat provision etc.

4. Find the internal diameter of the heater tube d_e such that τ =1 with the assumption that the external heat transfer coefficient at the heater is greater than or equal to 10 W/m^{2}K and a target efficiency from the Fig. 4.11.

5. From the value of chosen target efficiency from the η vs τ plot, the required power output and the required rate of heat input is calculated.

6. Now the designer is left with finding out the number of tubes required for heater. For this, a plot of heat flux (Q_{in} in W/m^2) v/s 1/τ is used. Figure 4.13 shows the values of heat flux to working fluid obtained from CFD plotted against 1/τ which follows an empirical relation obtained from regression analysis as given below.

$$Q_{in} = 400(\tau)^{0.7} \tag{4.3}$$

For the chosen value of τ the value of heat flux is found out from the eq. 4.3. From this, surface area required for the heater is calculated from which the number of tubes required could be arrived at.

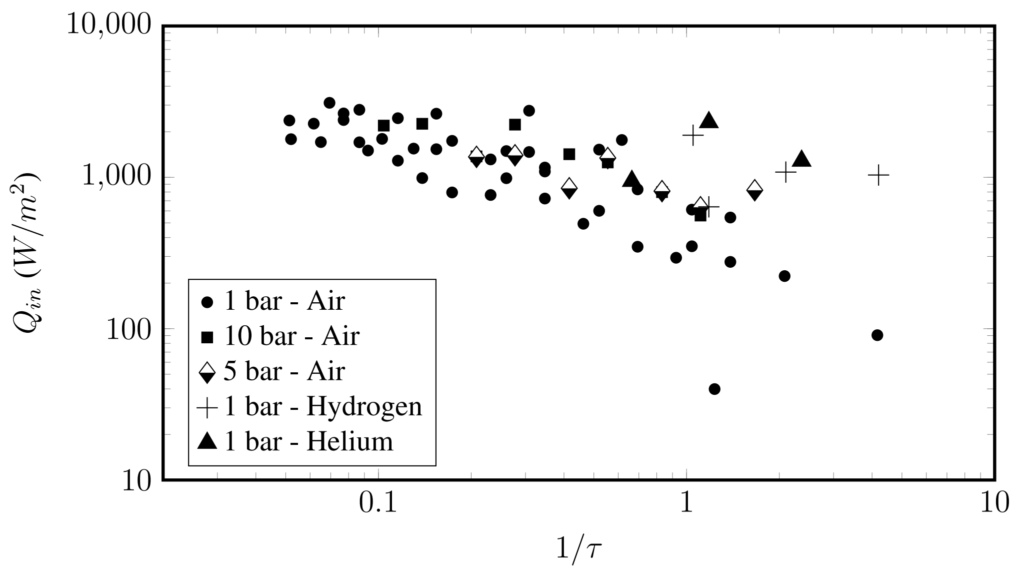

Figure 4.13: Variation of heat flux with 1/τ

The above design procedure bears some similarity to the one proposed by Organ (2013). But the advantage of the above procedure is that the range of τ is specified and the role of external heat transfer is clearly brought out. A target efficiency can be easily read from the Fig. 4.11 as opposed to making series of guesses in Organ's work. This helps in avoiding over or under design of the heater by choosing unrealistic values of efficiencies.

4.4 Summary

The non dimensional number τ has been characterized and has been shown to be useful in the design of Stirling engines, specifically the heater exchanger. Since the number covers almost all the parameters that are required for designing a Stirling engine, it is shown that this dimensional group can predict the performance of a given heater design and operating conditions. Along with Beale number the new non-dimensional number (τ) can be used to design and assess the performance of the heater heat exchanger. A design sequence for the heater is proposed for a quick back-of-the-envelop calculation.

CHAPTER 5

Conclusions

This thesis has contributed to the fundamental experimental and computational investigation on design of Stirling engines, and in particular the design of heater. Its contributions are both at a level of improving the understanding and clarifying issues around conflicting features in literature as well as providing a new design procedure for the first approximation of the dimensions of the heater.

A Stirling engine is a complex thermodynamic system even though it is simple in construction as compared to other engines. One of the basic takeaways from this thesis is that the design corresponding to the external flow over the heat exchangers is as important as the design for the internal flow. This is something that is given very little attention in the literature. It is shown that increasing the charge pressure and/or change of working fluid will not always guarantee an improvement in the performance of the engine. A single non dimensional number, τ, defined as the ratio of conduction to convection time scales, identified here is sufficient to capture the engine performance characteristics for a range of operating pressures, speeds, geometry and working fluids. It is also shown that this non dimensional number controls the phase difference between pressure and heat input without the need for change of the phase angle between the pistons. The phase angle of 90° is not necessarily the optimum which is a generally accepted value in the literature. This thesis proposes a new procedure for design of Stirling engine for domestic power application. The two non-dimensional numbers namely, the Beale number and τ are useful tools in the first approximation of the design of the engine.

The following conclusion can be made based on the experimental investigation and numerical simulations of Stirling engine from the current work -

- Detailed heat exchanger performance measurements and motoring tests were conducted on the lab engine. The results were used in setting up the CFD simulations.
- The 2D axi-symmetric model is shown to be a useful model in determining the performance of the engine.

- A new non-dimensional group τ, which is the ratio of conductive to convection time scale, is proposed using dimensional analysis and shown to capture the engine performance variation for a range of operating conditions and working fluids.
- The expansion and compression are shown to be broadly in phase with heat addition and heat rejection respectively when $\tau = 1$ and hence leading to optimal performance.
- The importance of using the new non dimensional group τ in addition to Baele number is brought out.
- A design sequence for the engine is proposed for a quick back-of-the-envelop calculation.
- An engine with a new design can be fabricated from the insights gained form this thesis.

Some suggestions and future work

An engine that can produce a shaft power of 200 - 250 W can be built when some fabrication and mechanical aspects of the design are further improved. It was observed in the experiments that the frictional power in the engine is on the higher side and steps must be taken to reduce the friction in the engine. Since combustion gases do not enter the piston-cylinder arrangement, solid lubrication can be used instead of oil lubrication avoiding regular change of the oil. A deeper analysis of different types of piston crank mechanisms and configurations of the engine is needed to reduce the frictional power and better dynamic balancing of the engine. Since for any meaningful power output, the engine must be pressurized, provisions for hermetic sealing in the engine must be made and associated dynamic seals must be installed. To keep the external heat transfer coefficient in the heater on the higher side, a good external flow design must be made by adding baffles etc. Innovation in the area of regenerator design is needed including in the areas of material, type of pores, manufacturing processes etc., to improve its effectiveness.

APPENDIX A

UDF for piston motion

A.1 Compression piston UDF

```
#include "udf.h"

#define r 0.03                  /* in meter */
#define l 0.12                  /* in meter */
#define omega_0 41.88790205     /* Constant rpm for cranking */
#define I 0.008717       /*Mass moment of Inertia kg m^2 */
#define A_1 0.002827433  /*Area of Piston */
#define A_2 0.002827433  /*Area of Piston */

static real th_n = 0.715584993;
static real omega_n = 0;
DEFINE_CG_MOTION(p1, dt, vel, omega, time, dtime)
{
        face_t f;
        Thread *t;
        real omega_np1, th_np1, force1, Pressure;
        float stroke;
        if (!Data_Valid_P ())
        return; /*Donot compute force if the solution is not initialized */
        t = DT_THREAD (dt);
        /*get the thread pointer (dt) corresponding to piston p1 for which the motion is defined*/
        /* Compute force on thr piston p1 using pressure and area */
        begin_f_loop(f,t)
        {
                Pressure = F_P(f,t);
        }
        end_f_loop(f,t)
        force1 = -(Pressure -101325)*A_1;
        if (time<100000)
        {
                omega_n = omega_0;
                th_np1 = th_n + omega_n*dtime;
        }
        else
        {
                omega_np1 = omega_n + Pressure*r*dtime/I*(A_1*sin(th_n) + A_2 * sin(th_n + 100*M_PI/180));
                th_np1 = th_n + omega_n*dtime;
                Message ("Pressure = %f, Force1 = %f\n", Pressure, force1);
        }
        stroke = sqrt(pow(l,2) - pow(r*sin(th_n),2));
        vel[0] = - r * sin(th_n) * (1 + r * cos(th_n)/stroke)  * (th_np1 - th_n) / dtime; /*Specify x velocity for piston 1*/
        th_n = th_np1;
        omega_n = omega_np1;
}
```

A.2 Expansion piston UDF

```
#include "udf.h"

#define r 0.03                  /* in meter */
```

```
#define l 0.12                    /* in meter */
#define omega_0 41.88790205       /* Constant rpm for cranking */
#define I 0.008717        /*Mass moment of Inertia kg m^2 */
#define A_1 0.002827433   /*Area of Piston */
#define A_2 0.002827433   /*Area of Piston */

static real th_n = 2.460914245;
static real omega_n = 0;

DEFINE_CG_MOTION(p2, dt, vel, omega, time, dtime)
{
face_t f;
Thread *t;
real omega_np1, th_np1, force2, Pressure;
float stroke;
if (!Data_Valid_P ())
return;                           /*Donot compute force if the solution is not initialized */
t = DT_THREAD (dt);               /*get the thread pointer (dt) corresponding to piston p1 for which the motion is defined*/
/* Compute force on thr piston p1 using pressure and area */
begin_f_loop(f,t)
{
Pressure = F_P(f,t);
}
end_f_loop(f,t)
force2 = (Pressure -101325)*A_2;
if (time<100000)
{
omega_n = omega_0;
th_np1 = th_n + omega_n*dtime;
}
else
{
omega_np1 = omega_n + Pressure*r*dtime/I*(A_1*sin(th_n) + A_2 * sin(th_n + 100*M_PI/180));
th_np1 = th_n + omega_n*dtime;
Message ("Pressure = %f, Force1 = %f\n", Pressure, force2);
}
stroke = sqrt(pow(l,2) - pow(r*sin(th_n),2));
vel[0] = r * sin(th_n) * (1 + r * cos(th_n)/stroke) * (th_np1 - th_n) / dtime; /*Specify x velocity for piston 2*/
th_n = th_np1;
omega_n = omega_np1;
}
```

REFERENCES

1. **Alfarawi, S.**, **R. Al-Dadah**, and **S. Mahmoud** (2016). Influence of phase angle and dead volume on gamma-type stirling engine power using cfd simulation. *Energy Conversion and Management*, **124**, 130–140.

2. **Asnaghi, A.**, **S. Ladjevardi**, **P. Saleh Izadkhast**, and **A. Kashani** (2012). Thermodynamics performance analysis of solar stirling engines. *ISRN Renewable Energy*, **2012**.

3. **Batmaz, I.** and **S. Üstün** (2008). Design and manufacturing of a v-type stirling engine with double heaters. *Applied Energy*, **85**(11), 1041–1049.

4. **Birol, F.** (2015). World energy outlook 2015. *International Energy Agency*, **1**.

5. **Carlsen, H.**, **N. Ammundsen**, and **J. Traerup**, 40 kw stirling engine for solid fuel. *In Energy Conversion Engineering Conference, 1996. IECEC 96., Proceedings of the 31st Intersociety*, volume 2. IEEE, 1996.

6. **Carlson, H.**, **M. B. Commisso**, and **B. Lorentzen**, Maximum obtainable efficiency for engines and refrigerators based on the stirling cycle. *In 25th Intersociety Energy Conversion Engineering Conference*. 1990.

7. **Champier, D.**, **J.-P. Bédécarrats**, **T. Kousksou**, **M. Rivaletto**, **F. Strub**, and **P. Pignolet** (2011). Study of a te (thermoelectric) generator incorporated in a multifunction wood stove. *Energy*, **36**(3), 1518–1526.

8. **Chen, W.-L.**, **K.-L. Wong**, and **Y.-F. Chang** (2014). A computational fluid dynamics study on the heat transfer characteristics of the working cycle of a low-temperature-differential γ-type stirling engine. *International Journal of Heat and Mass Transfer*, **75**, 145–155.

9. **Cheng, C.-H.**, **H.-S. Yang**, and **L. Keong** (2013). Theoretical and experimental study of a 300-w beta-type stirling engine. *Energy*, **59**, 590–599.

10. **Cheng, C.-H.** and **Y.-J. Yu** (2010). Numerical model for predicting thermodynamic cycle and thermal efficiency of a beta-type stirling engine with rhombic-drive mechanism. *Renewable Energy*, **35**(11), 2590–2601.

11. **Cinar, C.** and **H. Karabulut** (2005). Manufacturing and testing of a gamma type stirling engine. *Renewable energy*, **30**(1), 57–66.

12. **Costa, S.**, **I. Barreno**, **M. Tutar**, **J. Esnaola**, and **H. Barrutia** (2015). The thermal non-equilibrium porous media modelling for cfd study of woven wire matrix of a stirling regenerator. *Energy Conversion and Management*, **89**, 473–483.

13. **Duan, C.**, **C. Sun**, **S. Shu**, **G. Ding**, **C. Jing**, and **J. Chang** (2015). Similarity design and experimental investigation of a beta-type stirling engine with a rhombic drive mechanism. *International Journal of Energy Research*, **39**(2), 191–201.

14. **Dyson, R. W.**, **S. M. Geng**, **R. C. Tew**, and **M. Adelino** (2008). Towards fully three-dimensional virtual stirling convertors for multi-physics analysis and optimization. *Engineering Applications of Computational Fluid Mechanics*, **2**(1), 95–118.

15. **Dyson, R. W.**, **S. D. Wilson**, **R. C. Tew**, and **R. Demko**, Fast whole-engine stirling analysis. *In Proceedings of 3rd International Energy Conversion Engineering Conference*. 2005*a*.

16. **Dyson, R. W.**, **S. D. Wilson**, **R. C. Tew**, and **R. Demko**, Stirling analysis comparison of commercial vs. high-order methods. *In Third IECEC*. 2005*b*.

17. **Ernst, W. D.** and **R. K. Shaltens** (1997). Automotive stirling engine development project. Technical report, NASA CR-190780.

18. **FINKELSTEIN, T.**, Generalized thermodynamic analysis of stirling engines. *In SAE Technical Paper*. SAE International, 1960. URL `http://dx.doi.org/10.4271/600222`.

19. **Formosa, F.** and **G. Despesse** (2010). Analytical model for stirling cycle machine design. *Energy Conversion and Management*, **51**(10), 1855–1863.

20. **Gheith, R.**, **F. Aloui**, **M. Tazerout**, and **S. Ben Nasrallah** (2012). Experimental investigations of a gamma stirling engine. *International journal of energy research*, **36**(12), 1175–1182.

21. **Hirata, K.**, **S. Iwamoto**, **F. Toda**, and **K. Hamaguchi**, Performance evaluation for a 100 w stirling engine. *In Proceedings of Eighth International Stirling Engine Conference*. 1997.

22. **Hoshino, T.**, **H. Naito**, **T. Fujihara**, and **K. Eguchi**, Experimental study on stirling engine generator and solar receiver system for future space applications. *In Energy Conversion Engineering Conference and Exhibit, 2000.(IECEC) 35th Intersociety*, volume 1. IEEE, 2000.

23. **Ibrahim, M. B.**, **M. Mittal**, **T. Simon**, and **D. Gedeon**, A 2-d cfd model of a free piston stirling engine for space applications with annular heat exchangers. *In AIAA 2nd International Energy Conversion Engineering Conference Providence, RI*. 2004.

24. **Iwamoto, S.**, **K. Hirata**, and **F. Toda** (2001). Performance of stirling engines. arranging method of experimental results and performance prediction. *JSME International Journal Series B Fluids and Thermal Engineering*, **44**(1), 140–147.

25. **Kagawa, N.**, An experimental study of a 3-kw stirling engine. *In Energy Conversion Engineering Conference and Exhibit, 2000.(IECEC) 35th Intersociety*, volume 1. IEEE, 2000.

26. **Karabulut, H.** (2011). Dynamic analysis of a free piston stirling engine working with closed and open thermodynamic cycles. *Renewable Energy*, **36**(6), 1704–1709.

27. **Karabulut, H.**, **H. S. Yücesu**, **C. Çınar**, and **F. Aksoy** (2009). An experimental study on the development of a β-type stirling engine for low and moderate temperature heat sources. *Applied Energy*, **86**(1), 68–73.

28. **Karabulut, H.**, **H. S. YÜCESU**, and **A. KOCA** (2000). Manufacturing and testing of a v-type stirling engine. *Turkish Journal of Engineering and Environmental Sciences*, **24**(2), 71–80.

29. **Kelm, G.**, **J. Cairelli**, and **R. Walter** (1981). Test results and facility description for a 40-kilowatt stirling engine. Technical report, National Aeronautics and Space Administration, Cleveland, OH (USA). Lewis Research Center.

30. **Kongtragool, B.** and **S. Wongwises** (2007). Performance of low-temperature differential stirling engines. *Renewable Energy*, **32**(4), 547–566.

31. **Kumar, S.**, **P. Paul**, and **H. Mukunda** (2007). Prediction of flame liftoff height of diffusion/partially premixed jet flames and modeling of mild combustion burners. *Combustion Science and Technology*, **179**(10), 2219–2253.

32. **Lane, N.**, **D. Berchowitz**, **D. Shade**, and **A. Karandikar**, Development of a high frequency stirling engine-powered 3 kw (e) generator set. *In Energy Conversion Engineering Conference, 1989. IECEC-89., Proceedings of the 24th Intersociety*. IEEE, 1989.

33. **Lertsatitthanakorn, C.** (2007). Electrical performance analysis and economic evaluation of combined biomass cook stove thermoelectric (bite) generator. *Bioresource technology*, **98**(8), 1670–1674.

34. **Mahkamov, K.** (2006*a*). An axisymmetric computational fluid dynamics approach to the analysis of the working process of a solar stirling engine. *Journal of solar energy engineering*, **128**(1), 45–53.

35. **Mahkamov, K.** (2006*b*). Design improvements to a biomass stirling engine using mathematical analysis and 3d cfd modeling. *Journal of Energy Resources Technology*, **128**(3), 203–215.

36. **Martaj, N.**, **L. Grosu**, and **P. Rochelle** (2007). Thermodynamic study of a low temperature difference stirling engine at steady state operation. *International Journal of Thermodynamics*, **10**(4), 165–176.

37. **Martini, W. R.**, *Stirling engine design manual*. US Department of Energy, Office of Conservation and Solar Applications, Division of Transportation Energy Conservation, 1978.

38. **Mastbergen, D.**, *Development and optimization of a stove-powered thermoelectric generator*. ProQuest, 2008.

39. **Mukunda, H. S.** (2003). Low cost, high efficiency biofuel-to-electricity, past and future. URL `http://cgpl.iisc.ernet.in/site2/Portals/0/Publications/General/LowCostBiofuelPowerpack2003.pdf`.

40. **Nuwayhid, R.**, **D. Rowe**, and **G. Min** (2003). Low cost stove-top thermoelectric generator for regions with unreliable electricity supply. *Renewable energy*, **28**(2), 205–222.

41. **Organ, A. J.**, *Stirling Cycle Engines: Inner Workings and Design*. John Wiley & Sons, 2013.

42. **Prieto, J.**, **J. Fano**, **R. Diaz**, and **M. González** (1994). Application of discriminated dimensional analysis to the kinematic stirling engine. *Proceedings of the Institution of Mechanical Engineers, Part C: Journal of Mechanical Engineering Science*, **208**(5), 347–353.

43. **Prieto, J.**, **M. González**, **C. González**, and **J. Fano** (2000). A new equation representing the performance of kinematic stirling engines. *Proceedings of the Institution of Mechanical Engineers, Part C: Journal of Mechanical Engineering Science*, **214**(3), 449–464.

44. **Salazar, J. L.** and **W.-L. Chen** (2014). A computational fluid dynamics study on the heat transfer characteristics of the working cycle of a β-type stirling engine. *Energy Conversion and Management*, **88**, 177–188.

45. **Schmidt, G.** (1871). Theorie der lehmannschen calorischen maschine. *Zeit Des Vereines deutsch Ing*, **15**(1-12), 97–112.

46. **Snyman, H.**, **T. Harms**, and **J. Strauss** (2008). Design analysis methods for stirling engines. *Journal of Energy in Southern Africa*, **19**(3), 4–19.

47. **Takizawa, H.**, **N. Kagawa**, **A. Matsuguchi**, and **S. Tsuruno**, Performance of new matrix for stirling engine regenerator. *In Energy Conversion Engineering Conference, 2002. IECEC'02. 2002 37th Intersociety*. IEEE, 2004.

48. **Thombare, D.** and **S. Verma** (2008). Technological development in the stirling cycle engines. *Renewable and Sustainable Energy Reviews*, **12**(1), 1–38.

49. **Thorsen, J. E.**, **J. Bovin**, and **H. Carlsen**, 3 kw stirling engine for power and heat production. *In Energy Conversion Engineering Conference, 1996. IECEC 96., Proceedings of the 31st Intersociety*, volume 2. IEEE, 1996.

50. **Timoumi, Y.**, **I. Tlili**, and **S. B. Nasrallah** (2008). Design and performance optimization of gpu-3 stirling engines. *Energy*, **33**(7), 1100–1114.

51. **Tlili, I.** and **A. SaâĂŹed** (2013). Thermodynamic evaluation of a second order simulation for yoke ross stirling engine. *Energy Conversion and Management*, **68**, 149–160.

52. **Urieli, I.** and **D. M. Berchowitz**, *Stirling cycle engine analysis*. Taylor & Francis, 1984.

53. **Varunkumar, S.** (2012). *Packed bed gasification/combustion of biomass*. Ph.D. thesis.

54. **Walker, G.**, *Stirling-cycle machines*. Oxford University Press, 1973.

55. **Zhang, Z.** and **M. Ibrahim**, Development of cfd model for stirling engine and its components. *In 2nd International Energy Conversion Engineering Conference*, volume 2. 2004.

LIST OF PAPERS BASED ON THESIS

1. **Ajey Nagarkatti, Varunkumar. S,** Coupled Dimensional analysis and Computational Fluid Dynamics approach to design of alpha-type Stirling engines. *Proceedings of the 17th ISEC (International Stirling Engine Conference)*, Northumbria University, Newcastle, United Kingdom, August 2016.